Comparing Classical and Metaheuristic Methods to Optimize Multi-Objective Operation Planning of District Energy Systems Considering Uncertainties

Zahra Ghaemi[a,*], Thomas T. D. Tran[b], Amanda D. Smith[a]

[a] *Department of Mechanical Engineering, University of Utah, Salt Lake City, UT 84112, USA*
[b] *College of Engineering, Indiana Institute of Technology, Fort Wayne, IN 46803, USA*

Abstract

District energy systems (DES) can reduce CO_2 emissions associated with buildings while meeting the energy needs of a group of buildings with fossil fuel or renewable energy resources that are located on-site. One of the present challenges of DES is optimizing the operation of energy components, as different optimization methods are available. These optimization methods can have various requirements for implementation, distinct needs for engineering labor, and may rely on freely accessible software or proprietary software. Most importantly, different methods may result in dissimilar operation planning for a given DES, which makes the selection of optimization method a key consideration for decision-makers. In this study, two optimization methods, a mixed-integer linear programming (MILP) solver as a classical method and a non-dominated sorting genetic algorithm II (NSGA-II) as a metaheuristic method, are used to optimize the early-stage operation planning of a hypothetical DES for a university campus in a cool and dry climate. The objective is to minimize the operating cost and CO_2 emissions when considering uncertainties in energy demands, solar irradiance, wind speed, and annualized electricity-related emissions. Both methods present similar operation of energy components, operating cost, and operating CO_2 emissions. The MILP solver and NSGA-II algorithm vary in computation time to perform the optimization, initial knowledge to run the simulation, accessibility (free/open-source status), and satisfaction of constraints. This work compares the characteristics of a MILP solver and NSGA-II algorithm to help future researchers select the suitable optimization method related to their case study. The software underlying this work is open-source and publicly available to be reused and customized for early-stage operation planning of their specific DES. This work is novel by optimizing the operation planning of a mixed-used DES to minimize the cost and CO_2 emissions while considering uncertainties in weather parameters, energy demands, and annualized electricity-related emissions.

Keywords: optimization, distributed energy systems, open-source, NSGA-II algorithm, MILP solver, operation planning

Nomenclature

A_{surf}	Available surface area of solar PV system (m^2)
A_{swept}	Swept area of wind turbines (m^2)
β	Tilt angle of solar arrays (deg)
CHP	Combined heating and power
CV	Coefficient of variation
DES	District energy systems
EIA	Energy information administration

*Corresponding Author
Email address: zahra.ghaemi8@gmail.com (Zahra Ghaemi)

E_{coal} Electricity generated from coal (MWh)

E_{NG} Electricity generated from natural gas (MWh)

E_{RE} Electricity generated from renewable energy resources (MWh)

E_{total} Total electricity generation (MWh)

EF Emission factor

EF_{NG} Natural gas emission factor

EGEF Electricity generation emission factor

$EGEF_{coal}$ Electricity generation emission factor of coal

$EGEF_{NG}$ Electricity generation emission factor of natural gas

$EGEF_{fuel-mix}$ Electricity generation emission factor related to the fuel mix

$EGEF_{RE}$ Electricity generation emission factor of renewable energy resources

$EGEF_{RE-UU}$ Electricity generation emission factor of renewable energy resources purchased at the UU due to the renewable contract

$E_{gen,r,h}$ Sum of the electricity (kWh) that comes from the CHP system, solar PV, wind turbines, batteries, and the grid to buildings in each hour (h) of the representative days (r)

$E_{bat,t}$ Electricity stored in batteries (kWh) during time step t

$E_{bat,r,h}$ Electricity stored in batteries in each hour (h) of the representative days (r) (kWh)

E_{demand} Sum of the electricity demand (kWh) of buildings in each hour (h) of the representative days (r)

$E_{solar,r,h}$ Electricity generated from the solar PV system (kWh) in each hour (h) of the representative days (r)

$E_{wind,r,h}$ Electricity generated from the wind turbines (kWh) in each hour (h) of the representative days (r)

$E_{dis-bat,r,h}$ Discharging energy flow from the batteries (kWh) to the buildings in each hour (h) of the representative days (r)

$E_{ch-bat,r,h}$ Charging energy flow from renewables (kWh) to the batteries in each hour (h) of the representative days (r)

$E_{grid,r,h}$ Electricity purchased from the grid (kWh) in each hour (h) of the representative days (r)

$EMIS_{min}$ The corner point of the Pareto front, where CO_2 emissions are minimum (cost is maximum)

$EMIS_{max}$ The corner point of the Pareto front, where CO_2 emissions are maximum (cost is minimum)

E_{rated} Rated power of wind turbines (kW)

η_{boiler} Thermal efficiency of boilers

$\eta_{CHP,elect}$ Electrical efficiency of the CHP system

$\eta_{CHP,total}$ Total thermal efficiency of the CHP system

η_{ch} Charging efficiency of batteries

η_{dis} Discharging efficiency of batteries

$\eta_{inverter}$ Efficiency of inverters of solar PV system

η_{module} Efficiency of modules of solar PV system

F_{CHP} Total fossil fuel consumption of the CHP system (kWh)

$F_{CHP,r,h}$ Natural gas consumption of the CHP system in each hour (h) of the representative days (r) (kWh)

$F_{boilers,r,h}$ Natural gas consumption of boilers in each hour (h) of the representative days (r) (kWh)

GLPK GNU linear programming kit

$G_{T,r,h}$ Global tilted irradiance (kWh/m^2) in each hour (h) of the representative days (r)

MCMC Monte Carlo Markov chain

MILP Mixed-integer linear programming

NSGA-II Non dominated sorting genetic algorithm II

$O\&M$ Operation and maintenance

$O\&Mvar_i$ Variable O&M cost of energy components per energy unit ($/kWh)

$O\&Mfixed_i$ Fixed O&M cost of energy components per energy unit per year ($/kW-y)

$OPC_{r,h}$ Operating cost ($) of the DES in each hour (h) of the representative days (r)

$OPE_{r,h}$ Operating CO_2 emissions (kg-CO_2 emissions) of the DES in each hour (h) of the representative days (r)

P_{NG} Natural gas price ($/kWh)

P_{elect} Electricity price ($/kWh)

PDF Probability distribution function

PV Photovoltaic

$Q_{demand,r,h}$ Sum of the hot water demand (kWh) of buildings in each hour (h) of the representative days (r)

$Q_{gen,r,h}$ Sum of the hot water generation (kWh) of the CHP system and natural gas boilers in each hour (h) of the representative days (r)

STD Standard deviation

UU University of Utah

$V_{wind,r,h}$ Wind velocity (m/s) in each hour (h) of the representative days (r)

$V_{wind,rated}$ Rated wind velocity (m/s) of wind turbines

V_{ci} Cut-in wind velocity (m/s) of wind turbines

V_{co} Cut-off wind velocity (m/s) of wind turbines

1. Introduction

Residential and commercial buildings are significant energy users, being responsible for 27% of natural gas consumption and 70% of electricity consumption in the U.S. (Energy Information Administration (EIA), 2021). Due to their high level of energy consumption, buildings are an important target for emission mitigation in cities, neighborhoods, and campuses.

District energy systems (DES) can reduce emissions associated with buildings (Alarcon-Rodriguez et al., 2010). The role of the DES is to provide heating and electricity to campuses, neighborhoods, or a group of buildings efficiently using a combination of energy sources located on-site and electricity purchased from the grid.

One of the challenges in the development of a DES is the evaluation and optimization of operation planning (Mahmoud et al., 2020) as various optimization methods are present. The implementation and engineering labor of optimization methods are distinct. To use some methods, a user may buy expensive proprietary software. More importantly, using different optimization methods may result in dissimilar operation planning for a given DES. Therefore, comparing the results and performance of optimization methods on a DES is necessary for selecting a suitable optimization method in a case study.

Several review studies are available in the literature that investigate optimizing the operation planning of DES, hybrid renewable energy systems, microgrids, and distributed energy systems. Optimization methods in these energy systems are mainly categorized into classical methods and metaheuristic algorithms (Alarcon-Rodriguez et al., 2010; Banos et al., 2011; Bagherian et al., 2021):

1. *Classical methods:* Classical methods are widely used to optimize the operation planning of DES (Bagherian et al., 2021) using analytical calculations, as they can find near-optimum solutions. Classical methods consist of weighted-sum methods and Pareto-based optimization methods. The weighted-sum method combines all objectives into one mathematical function, where relative weights determine the relative importance of each objective (Banos et al., 2011). Pareto-based optimization methods include generating a set of non-dominated solutions (e.g., ϵ-constraint). The weighted-sum method is limited as it is difficult to adjust the weight factors for different objectives. Therefore, the Pareto-based optimization methods are preferred to the weighted-sum methods (Banos et al., 2011).

2. *Metaheuristic algorithms:* Metaheuristic algorithms are computational intelligence algorithms mainly used to solve complex optimization problems (Abdel-Basset et al., 2018). Metaheuristic algorithms are used in a growing number of research papers that tackle the optimization of operation planning in DES (Banos et al., 2011). Typically, metaheuristic algorithms share four characteristics (Boussaïd et al., 2013): they are inspired by nature, they use stochastic/random variables, they have several parameters that need to be fitted to a problem, and they do not use derivatives to optimize a problem. Metaheuristic algorithms have the advantage of optimizing non-linear problems in addition to linear problems. They can be used for single-objective optimization such as genetic algorithm and multi-objective optimization such as non-dominated sorting genetic algorithm II (NSGA-II).

Researchers have discussed whether an optimization method is preferred to other methods in various fields, especially when the methods are from different categories (classical vs. metaheuristic). For example, Ab Wahab et al. (2020) compared the classical and metaheuristic methods when optimizing the robot motion planning. They concluded that implementing the metaheuristic methods resulted in superior performance (e.g., execution time and energy consumption of the robot) compared to the classical methods. Silveira et al. (2021) compared the classical and metaheuristic methods to optimize the configuration of distributed energy systems to minimize the power losses in the system. They concluded that classical methods achieved a better solution to minimize the power losses than the metaheuristic methods. As mixed opinions are present on using a classical method versus a metaheuristic method, guidance on selecting the method to optimize the operation planning of energy systems is needed.

Several studies are available that optimized the operation planning of energy systems using different methods (Ikeda and Ooka, 2015; Rasouli et al., 2019; Shen et al., 2020). However, the authors of these studies performed a single-objective cost optimization. Emissions are also considered as an objective in addition to cost by researchers when optimizing the operation planning of energy systems, as greenhouse gas emissions are the main contributor to climate change (e.g., Capone et al. (2021); Bastani et al. (2018); Moghaddam et al. (2012)). Cost is often inversely proportional to the emissions associated with a project. Therefore, a multi-objective optimization is necessary to represent the trade-off between cost and emissions and help operators and designers of DES with decision-making when conflicting objectives are present.

This literature review is focused on comparing different methods to optimize the multi-objective *operation planning* while acknowledging the various research papers that have optimized the *design* of energy systems and compared different optimization methods (Fazlollahi et al., 2012; Ghiasi, 2019; Jing et al., 2019; Guo et al., 2021; Cao et al., 2021; Xu et al., 2021).

Only two studies (Ullah et al., 2021; Wu et al., 2021) performed multi-objective optimizations of *operation planning* and compared different optimization methods. Ullah et al. (2021) showed the operating cost and emissions are higher in multi-objective particle swarm optimization compared to multi-objective genetic algorithm and multi-objective wind-driven optimization algorithm. Wu et al. (2021) compared the multiple group search optimization algorithm, multi-objective particle swarm optimization, and multi-factorial evolutionary algorithm I and II. They concluded that multi-factorial evolutionary algorithm II performed better than the other three multi-objective optimization methods regarding four (span, spread, hypervolume, and convergence) metrics. Both studies focused on metaheuristic algorithms and excluded the classical methods in their studies. They also set the energy demands, weather parameters, and electricity-related emissions to be constant values. However, in a real-world case study, changes in electricity and heating demands, intermittent solar irradiance and wind speed, and variabilities in electricity-related emissions due to changes in the electricity generation mix can affect the operation planning of energy systems. Therefore, it is necessary to consider the uncertainties in energy demands, weather parameters, and electricity-related emissions to optimize the multi-objective operation planning of energy systems (Dranka et al., 2021; Collins et al., 2017).

Many recent studies have considered the uncertainties in energy demands, weather parameters, and energy prices in single-objective (Li et al., 2019; Zhou et al., 2020; Yang and Su, 2021; Zhong et al., 2021) and multi-objective (Bornapour et al., 2017; Mafakheri et al., 2020; Yan et al., 2020; Zhao et al., 2020; Yang et al., 2020; Wang et al., 2021; Prabatha et al., 2021; Dini et al., 2022) optimization problems to plan the operation of energy systems. However, variabilities in electricity-related emissions are neglected in these studies. Electricity-related emissions can vary throughout the year due to the different efficiencies of power plants and various origins and sub-types of fossil fuels (Ghaemi and Smith, 2022). These variabilities of electricity-related emissions can affect the operation planning of a DES. It is especially important to consider these variabilities when emissions are quantified in an optimization problem (Mavromatidis et al., 2018a). Mavromatidis et al. (2018b,c) quantified the long-term changes in electricity-related emissions in optimizing the design of a DES by considering the evolution of the Swiss electricity generation mix in the future. To the best of our knowledge, no study has considered the effects of uncertainties in annualized electricity-related emissions on the operation planning of DES.

1.1. Motivations of This Study

Two research gaps are observed from the literature review to optimize the multi-objective operation planning of energy systems: first, no study considered the uncertainties in annualized electricity-related emissions, and second, no study has evaluated the effects of different optimization methods given the uncertainties.

This paper fills the two research gaps and provides practical guidance to optimize the multi-objective operation planning of a DES considering uncertainties in energy demands, solar irradiance, wind speed, and annualized electricity-related emissions. The objective is to minimize the operating cost and CO_2 emissions using a mixed-integer linear programming (MILP) solver and the NSGA-II method. The MILP solver and the NSGA-II algorithm are selected because they belong to the two main categories of optimization methods, classical method (MILP solver) and metaheuristic algorithm (NSGA-II algorithm). Also, these two methods are widely used to optimize the operation planning of energy systems (Pickering et al., 2016; Khezri and Mahmoudi, 2020; Bagherian et al., 2021).

Using the MILP method versus the NSGA-II algorithm involves advantages and limitations. Some studies stated that using the MILP method resulted in higher computation time compared to the NSGA-II algorithms (Arya, 2021), while other studies stated implementing the MILP method required less computation time compared to the NSGA-II algorithm (HA et al., 2017). In some studies, superior results are obtained when using NSGA-II algorithm compared to MILP method (Sun et al., 2019; Pooranian et al., 2016). Other studies declared the MILP method must be used to obtain the global optimum in an optimization problem (Mavromatidis et al., 2018c; Bagherian et al., 2021). Furthermore, implementing the NSGA-II algorithm is more complex, while it can solve more complex optimization problems compared to the MILP method (HA et al., 2017). Therefore, due to the mixed opinions and lack of fundamental knowledge when using the MILP method and NSGA-II algorithm for a DES under uncertainties, this study is focused on comparing the results and characteristics of the MILP method and NSGA-II algorithm when optimizing the operation planning.

The software underlying this work is open-source and publicly available so that it can be reused and customized for early-stage operation planning of a specific DES (Z. Ghaemi, A.D. Smith, 2021). An open-source framework is valuable in energy system research due to its role in improving the quality of science and having more effective collaboration with other researchers (Pfenninger et al., 2017). Moreover, it is important to present this study as an open-source framework because the lack of open-source tools is one of the main challenges in the modeling and optimization of energy systems (Klemm and Vennemann, 2021). In this open-source framework, users can change the location of the case study, energy demands, characteristics of energy components, and energy prices for an early-stage operation planning of their specific DES. This framework can also help DES planners evaluate the effects of uncertainties in energy demands, weather parameters, and annualized electricity-related emissions on the calculated operating cost and CO_2 emissions of their DES.

The novelty of this paper is in a comprehensive comparison of MILP method and NSGA-II algorithm for multi-objective optimization of a DES under uncertainties. The two methods are compared with respect to the results and characteristics of methods. We improved the uncertainty analysis upon the methods available in the literature by conducting, for the first time, an uncertainty analysis that considers the effects of each hour on the next hour and the time of the day in scenario generation for a DES. The uncertainty of electricity-related emissions is also evaluated in the uncertainty analysis for the first time in a DES. Furthermore, we

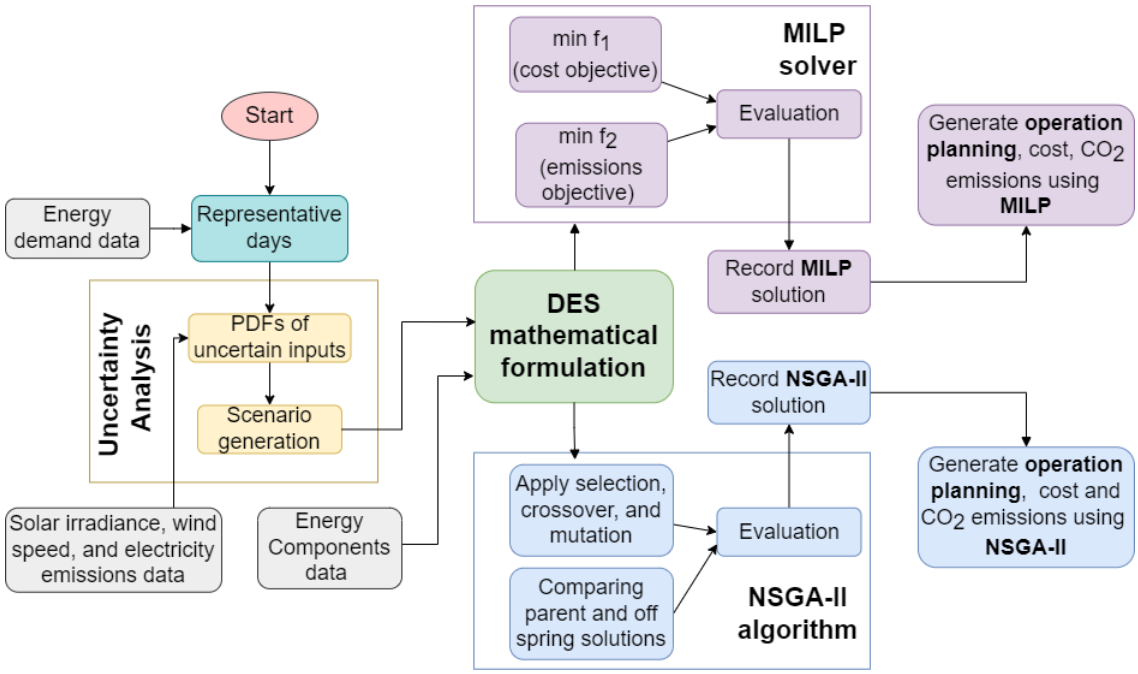

Figure 1: A framework to perform the multi-objective optimization under uncertainties by using two options for the optimization method: the MILP solver and NSGA-II algorithm.

provide an open-source framework implementing a multi-objective optimization of a DES under uncertainties, which can be reviewed, customized, and reused by others.

The key contributions of this work are summarized as follows:

1. Performing a multi-objective optimization to minimize the operating cost and CO_2 emissions of a multi-use DES under uncertainties in energy demands, solar irradiance, wind speed, and annualized electricity-related emissions for an early-stage analysis of a DES.

2. Comparing two methods, a MILP solver and NSGA-II algorithm, in multi-objective optimization of operation planning of a DES under uncertainties for a case study with respect to the computation time, ease of use, satisfaction of constraints, parallel computation, accessibility (open-source/free status), operation planning, operating cost, and operating CO_2 emissions.

3. Providing an open-source framework to optimize multi-objective operation planning of a DES under uncertainties for other case studies.

2. Methodology

In this study, a framework is presented to optimize the operation planning of a DES given the variabilities in energy demands, meteorological parameters, and electricity-related emissions by using two options for the optimization method, the MILP solver as a classical method and NSGA-II algorithm as a metaheuristic method (Figure 1). First, we describe a DES that uses fossil fuel and renewable resources that could provide the energy needs of a given group of buildings. We consider the variabilities in uncertain inputs (i.e., energy demands, meteorological parameters, and electricity-related emissions) by performing an uncertainty analysis to generate various yearly scenarios. Each scenario consists of the hourly variation of energy demands, meteorological parameters, and electricity-related emissions throughout a year. The yearly scenarios are used in the mathematical formulation of the DES to form the optimization problem. Two options, performing a MILP solver or NSGA-II algorithm, are presented to minimize the cost and CO_2 emissions in the operation planning of the DES. To reduce the computation time of the optimization, representative days are selected by performing a k-means clustering algorithm on energy demands. We use both methods separately for further comparison of the solutions and characteristics of the MILP solver and NSGA-II algorithm (Section 3).

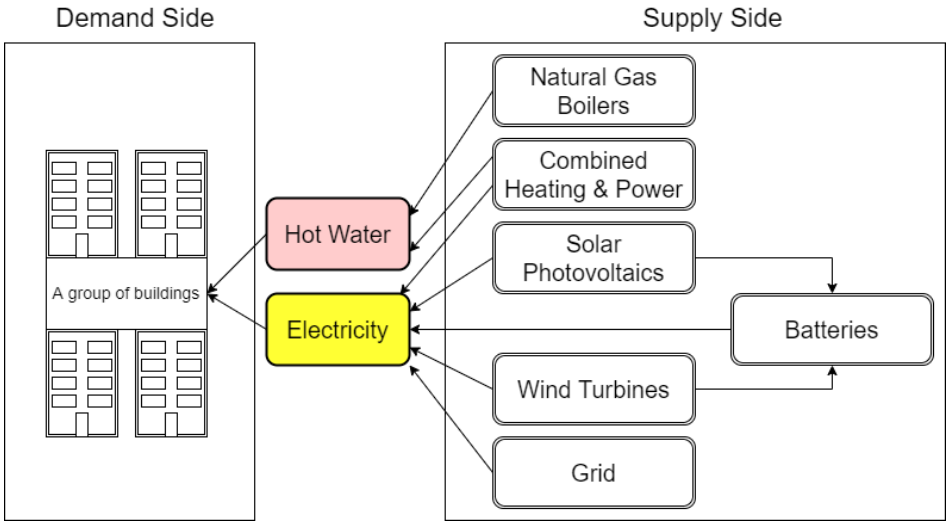

Figure 2: Schematic of the district energy system in this study

2.1. Description of District Energy System

In the hypothetical DES in this study, various energy components are selected to satisfy the energy demands of a group of buildings. The energy components of the DES consist of natural gas boilers, combined heating and power (CHP) system, solar photovoltaic (PV) system, wind turbines, and batteries, where these components do not physically exist in any location. Hence, we mathematically simulate these energy components to quantify their associated cost, emissions, and energy generation. We select a case study to use site-specific information and test the optimization framework with real-world data. The site-specific data of the case study are energy demands, energy prices, emission factors (EF), meteorological parameters, and rooftop areas. The selected case study consists of four buildings at the University of Utah (UU) in Salt Lake City in 2019. This site-specific data can be substituted in the open-source optimization framework (Z. Ghaemi, A.D. Smith, 2021) to test different locations and case studies.

The DES consisting of the demand side and supply side (Figure 2) is described in more detail in the following subsections:

2.1.1. Demand Side

The demand side of the DES consists of the hourly electricity and hot water demands of a group of buildings. The optimization algorithm must meet these energy demands in each hour by using the energy generated from the energy components and electricity purchased from the grid.

For the selected case study, the energy demands consist of the hourly electricity and hot water demands of four buildings at the UU in 2019. The characteristics of the four selected buildings at the UU are shown in Table 1. The energy demand quantities are collected from an extensive energy database for the UU that provides real-time electricity (kWh) and hot water (mmBTU) demands of the four selected buildings. The hot water demands (mmBTU) are quantified for the domestic hot water systems by measuring water inlet and outlet temperatures, flow rates, and assuming a constant specific heat for average water temperature and pressure at each time step. The hot water demands in mmBTU are converted to kWh to be consistent with the unit of electricity demands.

2.1.2. Supply Side

The supply side of the DES consists of various energy components that could provide the energy demands of the selected buildings. As multiple options of fossil fuel and/or renewable resources are available to generate electricity and hot water, first, we select the energy components of the DES. Then, we set the energy prices and EFs to quantify the operating cost and CO_2 emissions of the selected energy components. Finally, we quantify the sizing of energy components to evaluate the maximum capacities of the energy components in the operation planning of the DES.

Table 1: Characteristics of the selected four buildings at University of Utah in 2019

Building number	Space type	Floor area (m^2)	Total annual electricity demand (MWh)	Total annual hot water demand (MWh)
1	Class, lab, & office	15,700	796.94	603.57
2	Class, lab, & office	32,100	1265.98	560.3
3	Medical lab, & office	47,700	4376.27	294.48
4	Physical fitness & office	12,500	964.40	272.63

Selections of Energy Components: The hypothetical supply side consists of natural gas boilers, microturbine CHP system, solar PV system, wind turbines, batteries, and the electrical grid. These are the components that can be used to meet the energy demands of the group of buildings served by the DES, and the optimization algorithms select from these options to meet the energy demands in each hour.

The CHP system, solar PV system, and wind turbines are chosen in the supply side as the prevalent technologies for electricity generation of distributed energy systems (Schwartz et al., 2017). Additionally, we include natural gas boilers and the electrical grid in the supply side as the most common ways of providing hot water and electricity demands to buildings. Furthermore, due to the intermittent nature of electricity generation from renewable resources, batteries are included in the supply side to store the excess electricity generation from the renewables for later use on an hourly basis.

A battery control policy is applied to manage the charging and discharging flows by the batteries in each hour. If the electricity generated from renewable resources is higher than the electricity demand, the excess electricity is transmitted to batteries until batteries are fully charged. When the electricity generated from renewable resources and the CHP system is lower than the electricity demand, the electricity stored in batteries is used until the batteries reach their depth of discharge. After that, electricity is purchased from the electrical grid. The electricity generated from the CHP system is not considered to be stored in the batteries. This control policy is applied to batteries because the price of electricity is assumed constant throughout the year in our case study.

Energy Prices and Emission Factors: The electricity and natural gas prices and EFs are needed to quantify the operating cost and CO_2 emissions associated with operating the energy components. Electricity and natural gas prices are the projected average rates of electricity and natural gas from the UU utility rates (University of Utah Sustainability and Energy Management, 2020) (Table A.1). Electricity and natural gas prices are assumed constant throughout the year in the case study.

A natural gas EF evaluates the emissions released per unit of natural gas consumption (*kg emissions/MWh natural gas consumption*). The natural gas EF is obtained from the U.S. Environmental Protection Agency (2020) (Table A.1) to quantify the operating emissions related to the natural gas consumption of boilers and the CHP system.

An electricity generation emission factor (EGEF) quantifies the emissions released per unit of electricity generation (*kg emissions/MWh electricity generation*) (Ghaemi et al., 2021). The total electricity generation in Utah in 2019 came primarily from coal (65%), natural gas (24%), and renewable energy resources (solar thermal, solar PV, wind turbines, and hydroelectric) (10%) (U.S. EIA, 2021). The annualized $EGEF_{fuel-mix}$ represents the EGEF quantified from the fuel mix associated with electricity generation in Utah in 2019 (Equation 1):

$$EGEF_{fuel-mix} = \frac{E_{coal} \times EGEF_{coal} + E_{NG} \times EGEF_{NG} + E_{RE} \times EGEF_{RE}}{E_{total}} \quad (1)$$

where E_{total} is the total electricity generation (MWh), E_{coal} is the electricity generated from coal, E_{NG} is the electricity generated from natural gas (MWh), and E_{RE} is the electricity generated from renewable energy resources (MWh) in Utah in 2019. The $EGEF_{coal}$, $EGEF_{NG}$, $EGEF_{RE}$ are the EGEF of coal, natural gas, and renewable energy resources, respectively. We assume that emissions from the renewable energy resources are zero ($EGEF_{RE}$=0), and the annualized $EGEF_{fuel-mix}$ consists of the EGEF of coal and natural gas in Utah in 2019.

The electricity purchasing policy at the UU is applied to quantify the EGEF from the grid at the UU ($EGEF_{UU}$). The UU signed a contract to purchase 54% of its electricity from a geothermal power plant

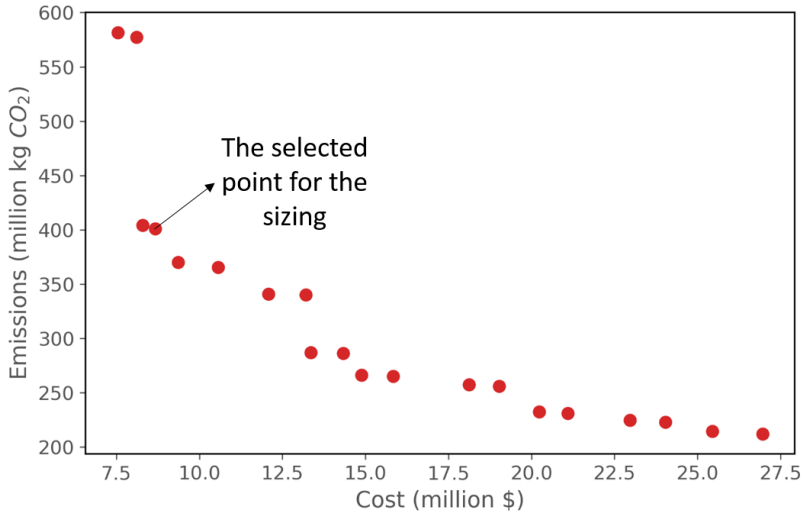

Figure 3: Cost and CO_2 emissions trade-off for different sizing of energy components. One point is selected from the Pareto front as the sizing of energy components in this study

in Nevada (Courtney Tanner, 2020). We use $EGEF_{fuel-mix}$ and assume 54% of the $EGEF_{fuel-mix}$ is associated with zero emissions due to the renewable contract at the UU. Hence, the $EGEF_{UU}$ is quantified as (Equation 2):

$$EGEF_{UU} = EGEF_{fuel-mix} \times (1 - 0.54) + EGEF_{RE-UU} \times 0.54 \tag{2}$$

where $EGEF_{RE-UU}$ is the EGEF of renewable energy resources purchased at the UU due to the renewable contract. The $EGEF_{RE-UU}$ is assumed to be zero in this study.

Only operating emissions are considered in the natural gas EF and EGEF, and the life cycle/embodied emissions of natural gas consumption and electricity purchased from the grid are neglected in this study. This is because of the limitations in the available life cycle methods (Islam et al., 2016) and the limitation in the available information related to the origins of consumed natural gas and purchased electricity in an early stage analysis of the DES. Such limitations in quantifying emissions can result in an inaccurate interpretation of life cycle emissions (Ghaemi and Smith, 2020).

Sizing of Energy Components: The sizing of energy components (i.e., the natural gas boilers, CHP system, solar PV system, wind turbines, and batteries) affects the maximum capacities of energy components in the operation planning of the DES. Therefore, optimizing the sizing of energy components is necessary to minimize the operating cost and CO_2 emissions in the operation planning. A two-stage stochastic optimization framework is used (Ghaemi et al., 2021) to select the capacities of energy components while providing the electricity and heating demand of buildings and minimize the total cost and operating emissions. A Pareto front is generated that shows the trade-off between the total cost and operating CO_2 emissions (Figure 3). Each point of this Pareto front represents a combination of the solar array areas, swept area of wind turbines, boilers capacity, CHP system capacity, and batteries capacity. The sizing of energy components are obtained from discrete values taken from the public database of energy companies (Tesla, 2021; Wind turbine database, 2021; Parker industrial boiler, 2021) or public technical reports (Gagnon et al., 2016; U.S. Department of Energy, 2016). One point from the Pareto front is selected which includes all of the available energy components in the DES and is closest to the minimum total cost. Because the first three points with a minimum total cost in the Pareto front do not use any wind turbine or battery, the fourth point with the minimum total cost is selected for the sizing of energy components (Figure 3). The sizing and characteristics of the selected point are shown in Table A.2 for natural gas boilers, Table A.3 for the microturbine CHP system, Table A.4 for the the solar PV system, Table A.5 for wind turbines, and Table A.6 for batteries.

2.2. Mathematical Formulation of District Energy System

In this subsection, the mathematical statements and equations needed to perform the multi-objective optimization of the natural gas boilers, CHP system, solar PV system, wind turbines, and batteries are presented to minimize the operating cost and CO_2 emissions. The decision variables are the natural gas consumption of the boilers ($F_{boilers,r,h}$ in kWh), natural gas consumption of the CHP system ($F_{CHP,r,h}$ in kWh), electricity stored in the batteries ($E_{bat,r,h}$ in kWh), and the electricity purchased from the electrical grid ($E_{grid,r,h}$ in kWh) in each hour (h) of the representative days (r).

Cost Objective: The first objective ($g_1(r)$) is minimizing the total operating cost for each representative day (Equation 3):

$$\begin{aligned} \text{Min } g_1(r) = &\text{ Min (Total Operating Cost for each Representative Day)} \\ = &\text{ Min } (\sum_{h=1}^{24} OPC_{r,h}), \end{aligned} \tag{3}$$

where $OPC_{r,h}$ is a matrix with 11 rows (number of representative days) and 24 columns (24 hours in each representative day) that holds the operating cost of the DES in each hour of the representative days. By summing the variable operating cost of the CHP, natural gas boilers, and the electrical grid, $OPC_{r,h}$ for each hour of the representative days is quantified (Equation 4):

$$\begin{aligned} OPC_{r,h} = &(\text{O\&M var}_{boilers} + P_{NG}) \times \text{F}_{boilers,r,h} + \\ &(\text{O\&M var}_{CHP} + P_{NG}) \times \text{F}_{CHP,r,h} + \\ &P_{elect} \times \text{E}_{grid,r,h} \end{aligned} \tag{4}$$

- $O\&Mvar_{boilers}$ is the variable O&M cost of the boilers per energy unit ($/kWh),
- P_{NG} is the natural gas price ($/kWh),
- $F_{boilers,r,h}$ is the natural gas consumption of boilers (kWh),
- $O\&Mvar_{CHP}$ is the variable O&M cost of the CHP system per energy unit ($/kWh),
- $F_{CHP,r,h}$ is the natural gas consumption of the CHP system (kWh),
- $E_{grid,r,h}$ is the electricity purchased from the grid (kWh), and
- P_{elect} is the electricity price ($/kWh) (Table A.1).

The variable cost ($OPC_{r,h}$) of the DES consists of the variable cost of the natural gas boilers, the CHP system, and the grid (Equation 4). This is because the variable cost of the solar PV system, wind turbines, and batteries is assumed to be zero (NREL, 2016a).

Emissions Objective: The second objective ($g_2(r)$) is to minimize the operating CO_2 emissions for each representative day (Equation 5):

$$\begin{aligned} \text{Min } g_2(r) = &\text{ Min (Total Operating Emissions for each Representative Day)} \\ = &\text{ Min } (\sum_{h=1}^{24} OPE_{r,h}) \end{aligned} \tag{5}$$

where $OPE_{r,h}$ is a matrix with 11 rows (number of representative days) and 24 columns (24 hours in each representative day) that holds the operating CO_2 emissions of the DES for each hour of the representative days. By summing the operating emissions of natural gas boilers, the CHP system, and the electricity from the grid, $OPE_{r,h}$ is quantified for each hour of the representative days (Equation 6):

$$\begin{aligned} OPE_{r,h} = &EF_{NG} \times \text{F}_{boilers,r,h} + \\ &EF_{NG} \times \text{F}_{CHP,r,h} + \text{EGEF} \times \text{E}_{grid,r,h} \end{aligned} \tag{6}$$

where EF_{NG} is the natural gas EF, and EGEF is the electricity generation EF (Table A.1).

Constraints: The hot water and electricity demands of buildings must be met in each hour of the representative days.

The $Q_{gen,r,h}$ holds the sum of the hot water generated (kWh) by the CHP system and natural gas boilers

for each hour of the representative days (Equation 7):

$$\begin{aligned} Q_{gen,r,h} &= \eta_{boiler} \times \mathrm{F}_{boilers,r,h} + (\eta_{CHP,total} - \eta_{CHP,elect}) \times \mathrm{F}_{CHP,r,h} \\ Q_{gen,r,h} &= Q_{demand,r,h} \end{aligned} \tag{7}$$

- η_{boiler} is the thermal efficiency of the boilers (Table A.2),
- $\eta_{CHP,total}$ is the total thermal efficiency of the CHP system, and
- $\eta_{CHP,elect}$ is the electrical efficiency of the CHP system (Table A.3).

The total thermal efficiency of the CHP system ($\eta_{CHP,total}$) is defined as the sum of the net power and net useful thermal output from the CHP system ($Q_{CHP} + E_{CHP}$) divided by the total fossil fuel consumption of the CHP system, $\eta_{CHP,total} = (Q_{CHP} + E_{CHP})/F_{CHP}$ (Darrow et al., 2017). The electrical efficiency of the CHP system ($\eta_{CHP,elect}$) is defined as the net generated electricity from the CHP system (E_{CHP}) divided by the total fossil fuel consumption of the CHP system, $\eta_{CHP,elect} = E_{CHP}/F_{CHP}$ (Kurnik et al., 2017). Equation 7 also shows that the hot water demand for each hour of the representative days ($Q_{demand,r,h}$) must be equal to the hot water generated (kWh) by the natural gas boilers and the CHP system ($Q_{gen,r,h}$)

The $E_{gen,r,h}$ (kWh) holds the sum of the net electricity from the batteries, the electricity purchased from the grid, and the electricity generated by the CHP system, solar PV system, and wind turbines to meet the electricity demand of all buildings for each hour of the representative days (Equation 8):

$$\begin{aligned} E_{gen,r,h} &= E_{dis-bat,r,h} - E_{ch-bat,r,h} + E_{grid,r,h} + \eta_{CHP,elect} \times \mathrm{F}_{CHP,r,h} + E_{solar,r,h} + E_{wind,r,h} \\ E_{gen,r,h} &= E_{demand,r,h} \end{aligned} \tag{8}$$

- $E_{dis-bat,r,h}$ is the discharging energy flow from the batteries to the buildings (kWh),
- $E_{ch-bat,r,h}$ is the charging energy flow from the renewables to the batteries (kWh),
- $E_{grid,r,h}$ is the electricity purchased from the grid (kWh),
- $E_{solar,r,h}$ is the electricity generated from the solar PV system (kWh), and
- $E_{wind,r,h}$ is the electricity generated from the wind turbines (kWh) (Table A.3).

Equation 8 also shows that the electricity demand for each hour of the representative days ($E_{demand,r,h}$) must be equal to the net electricity from the batteries, electricity purchased from the grid, and electricity generated by the CHP system and renewables ($E_{gen,r,h}$).

The electricity generated from the solar PV system ($E_{solar,r,h}$ in kWh) for each hour of the representative days can be quantified (Equation 9):

$$E_{solar,r,h} = \frac{A_{surf}}{\cos\beta} \times G_{T,r,h} \times \eta_{module} \times \eta_{inverter} \tag{9}$$

- A_{surf} is the available surface area for the solar PV system (m^2),
- β is the tilt angle of the solar arrays (deg),
- $G_{T,r,h}$ is the global tilted irradiance (kWh/m^2),
- η_{module} is the efficiency of modules, and
- $\eta_{inverter}$ is the efficiency of inverters (Table A.4).

It is estimated by NREL (2016b) that 60%–65% of commercial rooftop areas are suitable for solar PV deployment. Hence, the available surface area for the solar PV system (A_{surf} in m^2) is quantified as 60% of the total rooftop areas of the four selected buildings at the UU. The optimum tilt angle (β) is quantified using the NREL PVWatts calculator (Dobos, 2014). The PVWatts calculator is used to find the maximum electricity generated (kWh) by a commercial solar PV system when the tilt angle is a multiplier of five from 0 to 90 degrees (i.e.,0, 5, 10,..., 85, 90). The optimum β is quantified as *35* degrees for the case study's location, which is at 40.76 degrees latitude. The global tilted irradiance ($G_{T,r,h}$) is quantified using the Pvlib Python package (Holmgren et al., 2018, 2015) first to find the solar position in each hour and then evaluate the global irradiance on the tilted plate at 35 degrees. The direct normal irradiance, diffuse horizontal irradiance, and global horizontal irradiance are gathered from National Solar Radiation Database (Sengupta et al., 2018) to quantify the global tilted irradiance. The electricity generated from the solar PV system is limited by the power density of its modules (Table A.4) (Gagnon et al., 2016).

Various methods are available to quantify the electricity generated by wind turbines (Wang et al., 2019). Using the typical wind turbine power curve (Figure 4) is a suitable method when the power curve from the

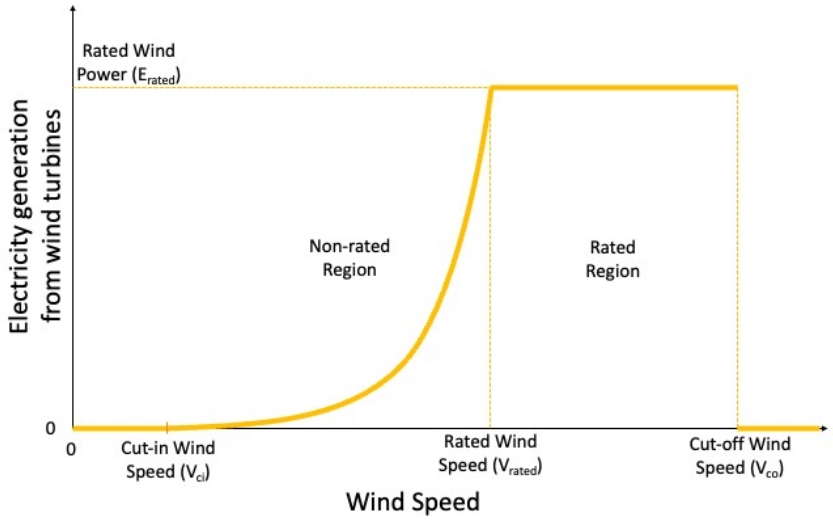

Figure 4: Typical wind power curve when the non-rated region is assumed to be non-linear (Dupont et al., 2018)

wind turbine manufacturer is unavailable. In the typical wind turbine power curve, no electricity is generated when the wind speed is less than the cut-in wind speed and more than the cut-off wind speed. Using the typical power curve, the electricity generated from the wind turbines ($E_{wind,r,h}$ in kWh) for each hour of the representative days can be quantified (Equation 10) (Nojavan et al., 2017a; Abbaspour et al., 2013):

$$E_{wind,r,h} = \begin{cases} 0 & V_{wind,r,h} < V_{ci} \\ E_{rated} \times \left(\frac{V_{wind,r,h} - V_{ci}}{V_{rated} - V_{ci}}\right)^3 \times \Delta t & V_{ci} < V_{wind,r,h} < V_{rated} \\ E_{rated} \times \Delta t & V_{rated} < V_{wind,r,h} < V_{co} \\ 0 & V_{wind,r,h} > V_{co} \end{cases} \tag{10}$$

- $V_{wind,r,h}$ is the wind velocity (m/s) for each hour of the representative days,
- V_{ci} is the cut-in wind velocity of wind turbines (m/s),
- E_{rated} is the rated power of wind turbines (kW),
- Δt is the time step (hour),
- $V_{wind,rated}$ is the rated wind velocity of wind turbines (m/s), and
- V_{co} is the cut-off wind velocity of wind turbines (m/s) (Table A.5).

The electricity stored in the batteries is quantified using the state of charge of batteries and their charging and discharging electricity flows. The amount of electricity stored in batteries during time step t ($E_{bat,t}$ in kWh) is (Equation 11):

$$E_{bat,t} = E_{bat,t-1} + \eta_{ch} \times E_{ch-bat} - E_{dis-bat}/\eta_{dis} \tag{11}$$

- $E_{bat,t-1}$ is the amount of electricity stored in batteries during time step t-1 (kWh),
- η_{ch} is the charging efficiency of the batteries,
- E_{ch-bat} is the charging electricity flow from renewables to batteries (kWh),
- η_{dis} is the discharging efficiency of the batteries, and
- $E_{dis-bat}$ is the discharging electricity flow from batteries to buildings (kWh) (Table A.6).

The percentage of the battery discharged compared to its total capacity must always be less than the depth of discharge of the battery. As the battery capacity is 54 kW and its depth of discharge is 90%, the discharged flow in an hour must be smaller than 48.6 kWh (=54kWh$\times$ 0.9) in this study.

2.3. MILP Optimization Solver

The problem that is formed in Subsection 2.2 with objective Equations 3 and 5 is a MILP problem. A MILP problem can be solved using optimization solvers. The most widely used MILP solvers for optimization include a general algebraic modeling system (GAMS), a mathematical programming language (AMPL), IBM ILOG CPlex optimization suite (Cplex, 2009), and GNU linear programming kit (GLPK) (Allegrini et al., 2015). The GLPK solver is a mathematical programming solver that can optimize linear programming and mixed-integer programming. In this study, we used the GLPK solver implemented by the Pyomo Python library (Hart et al., 2011, 2017) to optimize the MILP model for two reasons. First, the GLPK solver is one of the open-source/free MILP solvers, and second, it has shown success in optimizing the design and operation planning of energy systems (Zwickl-Bernhard and Auer, 2021; Alhamwi et al., 2019; Limpens et al., 2019)

The GLPK solver can perform a single-objective optimization. To perform a multi-objective optimization, ϵ-constraint method has been implemented (Jirdehi et al., 2017; Tabar et al., 2017) in the literature. We can perform the ϵ-constraint method in the following four steps (Wu et al., 2017):

1. A single-objective optimization is performed to minimize the operating cost of the energy components and find the corner point of the Pareto front, where cost is minimum and CO_2 emissions are maximum ($EMIS_{max}$).

2. Another single-objective optimization is performed to minimize the operating CO_2 emissions of the energy components and find the other corner point of the Pareto front, where CO_2 emissions are minimum ($EMIS_{min}$) and cost is maximum.

3. The difference between the maximum and minimum CO_2 emissions ($EMIS_{max}$-$EMIS_{min}$) is divided into n intervals, where n represents the number of points in the Pareto front (population size in Table 2).

4. The cost objective ($g_1(r)$ in Equation 3) is minimized while the CO_2 emissions objective ($g_2(r)$ in Equation 5) is treated as a constraint that should be less than and equal to the ϵ (Nojavan et al., 2017b). The mathematical form of the ϵ-constraint method is (Equation 12) (Wu et al., 2017):

$$\begin{aligned} &min\, g_1(r) \\ &g_2(r) \leq \epsilon_i \quad i \in 1, 2, ..., n-1 \\ &\epsilon_i = (i-1) \times (EMIS_{max} - EMIS_{min})/n + EMIS_{min} \quad i \in 1, 2, ..., n-1 \\ &\text{all the other constraints} \end{aligned} \tag{12}$$

2.4. NSGA-II Optimization Algorithm

The second method to optimize the operation planning of energy components is the NSGA-II algorithm. NSGA-II is a metaheuristic algorithm that has been used for the multi-objective optimization of the design and operation planning of energy systems (Amusat et al., 2018; Huang et al., 2019; Legorburu and Smith, 2020). NSGA-II optimization is performed in four main steps (Xu et al., 2020):

1. A random solution space is generated by assigning random values to decision variables, where continuous random values are obtained from the acceptable ranges of energy components. For example, the range of random variables assigned to the natural gas consumption of boilers must be from zero to the maximum natural gas consumption of boilers.

2. Solution sets are sorted, where each point is at least better in one objective (cost or emissions) compared to other points, and no point is superior in both cost and emissions, which are called non-dominated solutions. If a solution is superior in both cost and emissions, that would be the dominated and selected solution, and no Pareto front will be formed. This set of solutions is the parent set.

3. Using crossover and mutation concepts, offspring is created from the parent set.

4. This procedure iterates until the condition to end the program is met, and a Pareto front is formed.

Table 2: The set parameters to use in the MILP solver and NSGA-II algorithm

	Population size	Crossover probability	Crossover distribution index	Mutation probability	Mutation distribution index	Number of iterations
MILP	11	not required	not required	not required	not required	not required
NSGA-II	11	1	15	1	20	1000

In this study, the NSGA-II algorithm (Deb et al., 2002) is performed by using the Platypus library in Python (D. Hadka, 2019). The objective functions for the optimization problem are Equations 3 and 5.

Several trials are performed to evaluate the computation time, precision, and satisfaction of constraints of the system. Then, the parameters of the NSGA-II algorithm are set (Table 2). This table also shows that the NSGA-II algorithm requires more parameters compared to the MILP solver to optimize the operation planning of the DES.

In Table 2, the population size is selected as 11, which is the number of points in the Pareto front for both MILP and NSGA-II algorithm. The number of iterations is the most important parameter that affects the precision and satisfaction of constraints. For example, using 100 iterations resulted in an operating cost of $1868 for one day, and using 1000 iterations resulted in an operating cost of $1870 for a day. This is a small variability for the operating cost of a day when the number of iterations changes from 100 to 1000. However, when this variability sums up for a whole year, the results from the NSGA-II algorithm would be different from the MILP solver if iterations are fewer than 1000. The second important parameter is the mutation probability. The range of cost and emissions among the Pareto front points decreases by decreasing the mutation probability. Hence, we set the mutation probability to 1, the maximum available number, to obtain the maximum range of operating cost and emissions in the Pareto front. For example, when mutation probability is 1, the operating cost is from $1870 to $1895 in one day for different Pareto points, and when mutation probability is 0.2, the operating cost is from $1870 to $1872 in one day for different Pareto points. When the population size, number of iterations, and mutation probability are set, changing the crossover probability, crossover distribution index, and mutation distribution index does not affect the cost and emissions in each hour. Hence, these three are set as the default values for NSGA-II algorithm in Platypus library (D. Hadka, 2019).

2.5. Representative days

The annual optimization of the operation planning on an hourly basis is computationally expensive. To reduce the computational time, representative days (Scott et al., 2019) instead of the actual 365 days are used to optimize the operation planning of the DES. These representative days are selected by aggregating days with similar hourly energy demands into groups (Teichgraeber and Brandt, 2019; Van Der Heijde et al., 2019). Then, each group is represented by one day. We treat the representative days as though they are the actual days in the optimization problem. This is because the hourly energy demands throughout a year are only different by 2%–6% when using the representative days instead of actual days (Scott et al., 2019).

In this study, the k-means clustering algorithm selects the representative days. This method has been used in several studies in the literature related to multi-energy systems (Guo et al., 2021), integrated energy systems (Zhang et al., 2020), and DES (Fazlollahi et al., 2014).

To run a k-means algorithm, the number of clusters must be set, which is done by using the elbow method in this study (Marutho et al., 2018; Duong et al., 2019). The elbow method is performed by quantifying the inertia versus the number of clusters. Inertia is an indicator of the performance of the clustering algorithm (Yuan and Yang, 2019), which is the sum of distances of cluster members to their closest cluster center. At an elbow point, there is a significant change in the inertia value, but the inertia does not change extremely compared to the next point (Marutho et al., 2018). Figure 5 shows the inertia versus the number of clusters in this study. However, no significant change occurs from points 7 to 19 in the inertia, which requires a judgment call on the part of the authors. The typical number of clusters for k-mean algorithm is from 8–10 days (Schütz et al., 2018). Hence, point 9, a point within this range is selected. Selecting this point means that nine clusters are selected from the k-means clustering algorithm.

In this study, nine representative days are selected using the k-means clustering algorithm to partition the electricity and hot water demands of 365 days. Two additional representative days are added to these

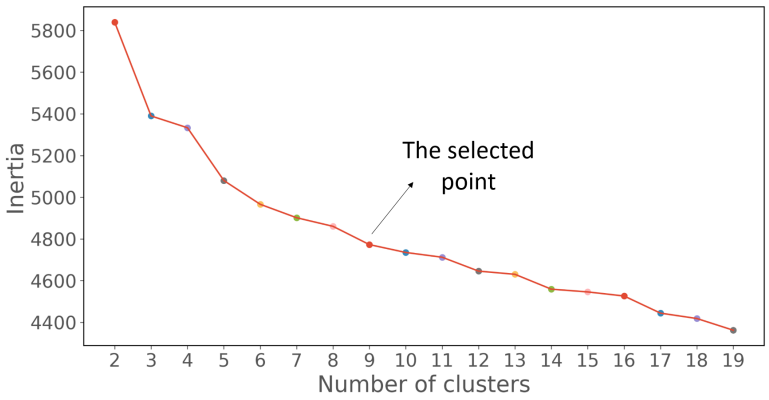

Figure 5: Elbow point is selected to quantify the optimum number of clusters in the k-means algorithm

nine representative days to include the days with extreme electricity and hot water demands, as the k-means clustering algorithm selects the average scenarios and not the extreme ones. The methodology to add these two additional representative days is directly adopted from Sun et al. (2014) and is also used by Mavromatidis et al. (2018c). Therefore, 11 representative days are selected using the k-means clustering algorithm for this study with assigned weight factors depending on the number of days that belong to each cluster center (Scott et al., 2019). The daily hot water and electricity demands of 365 actual days (small dots) and 11 representative days with their associated probability of occurrence (large dots) are shown in Figure 6. The probability of occurrence of each representative day is quantified as the number of days that belong to each cluster divided by the total number of days in the year. For example, 55 historical days within a year belong to the cluster of a representative day. The occurrence probability is quantified as 15.1%(=55/365 $\times$ 100). The sum of occurrence probability of all representative days is equal to 1, meaning each day of the year must belong to a cluster.

2.6. Uncertainty Analysis

In this study, uncertainties in electricity demand, hot water demand, solar irradiance, wind speed, and annualized EGEF are modeled to generate 10,000 yearly scenarios using a standard Monte Carlo Markov chain (MCMC).

These five uncertain inputs are selected because their variabilities can affect the operation planning of the DES. The electricity and hot water demands of buildings are variable due to the weather intermittency, changes in the occupancy, or adjustments in the schedules of electrical and mechanical systems in buildings (Urbanucci and Testi, 2018; Tran and Smith, 2019). The amount of electricity generated by the solar PV system and wind turbines varies due to the weather intermittency (Sharifzadeh et al., 2017; Karmellos et al., 2019). Also, electricity-related emissions are the most important driver of variabilities in emissions associated with a DES (Mavromatidis et al., 2018b). Therefore, electricity demand, hot water demand, solar irradiance, wind speed, and annualized EGEF are selected as the uncertain inputs for the uncertainty analysis.

To perform MCMC, the probability distribution function (PDF) of uncertain inputs are quantified:

- *PDFs of electricity demands and hot water demands:* To assess the PDFs of electricity and hot water demands, the variabilities in energy demands are captured for the representative days. First, for each representative day, the actual days that belong to the cluster of that representative day are gathered. Then, the electricity and hot water demands of actual days are collected and stored in arrays for each hour. Last, the values in each array are used to compute 528 (=11 representative days $\times$ 24 hours $\times$ 2 uncertain inputs) PDFs for electricity and hot water demands. The PDFs are generated using the available continuous distributions in the SciPy library (2019).

- *PDFs of solar irradiance and wind speed:* To assess the PDFs of solar irradiance and wind speed, the variabilities in weather parameters are captured over the years. First, for each representative day, the solar irradiance and wind speed actual data in Salt Lake City from 1998 to 2019 are gathered from the

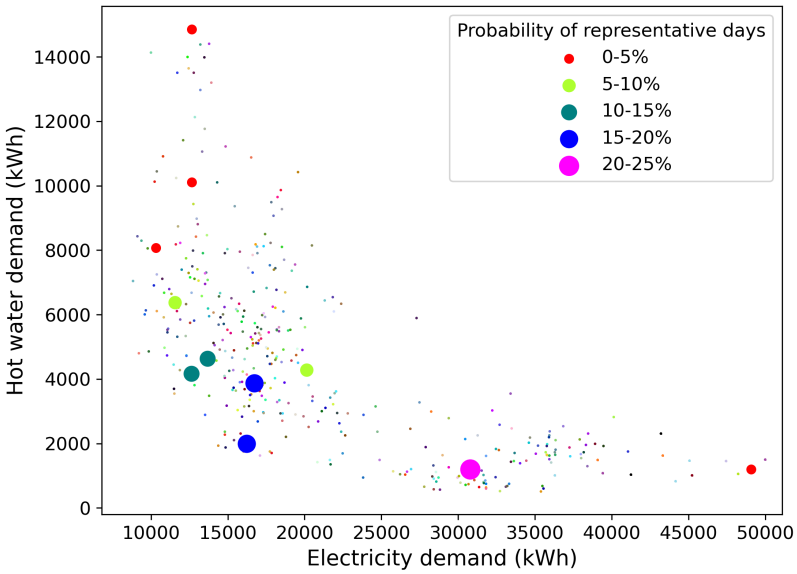

Figure 6: The daily hot water demands versus the electricity demands of 365 actual days (small dots) and 11 representative days with their associated probability of occurrence

National Solar Radiation Database (Sengupta et al., 2018). Then, the solar irradiance and wind speed values are collected and stored in an array for each hour. Twenty-two values are available for solar irradiance and wind speed from 1998 to 2019 (22 years) in each array. Last, these 22 actual values in each array are used to quantify 528 (=11 representative days × 24 hours × 2 uncertain inputs) PDFs for solar irradiance and wind speed. The PDFs are generated using the available continuous distributions in the SciPy library (2019).

- *PDF of annualized EGEF:* To assess the PDF of annualized EGEF, an uncertainty analysis method is used from Ghaemi and Smith (2022), where the annualized EGEF from Utah's fuel mix ($EGEF_{fuel-mix}$) is quantified using Equation 1. The $EGEF_{coal}$ and $EGEF_{NG}$ in Equation 1 are variable due to the presence of different sub-types/origins of fossil fuels and dissimilarities in the efficiencies of power plants (more details in Ghaemi and Smith (2022)). A PDF is generated from the variable annualized $EGEF_{fuel-mix}$ (Equation 1) by using the available continuous distributions in the SciPy library (2019). The PDF is a beta distribution for the annualized $EGEF_{fuel-mix}$ in Utah in 2019.

The PDFs of uncertain inputs are different for each day and hour of the day. Hence, as an example, we show the PDFs of electricity demand, heating demand, solar irradiance, wind speed, and EGEF for the first representative day at 12 pm (Figure 7).

After the PDFs of the five uncertain inputs are quantified, a procedure from Evans and Clausen (2015) is adopted to generate scenarios by implementing a standard MCMC method. In this method, scenarios for the energy demands, solar irradiance, wind speed, and annualized EGEF in each hour are only dependent on their values in the previous hour due to the first-order Markov chain rule. The standard MCMC method is performed in 6 steps for each uncertain input separately:

1. The PDF of the uncertain input in each hour is divided into 50 intervals, where the range of these 50 intervals is equal.

2. A matrix of size 50×50 ($M_{d,h}$) is formed for each hour (h) of the day (d) to quantify the transition probability of the uncertain input. The transition probability ($P_{i,j}$) is the number of transitions from the current interval (i) to the next selected interval (j) in each hour ($N_{i,j}$) divided by the total number of transitions (T) in each hour; $P_{i,j} = N_{i,j}/T$. The T value is the number of available data in each

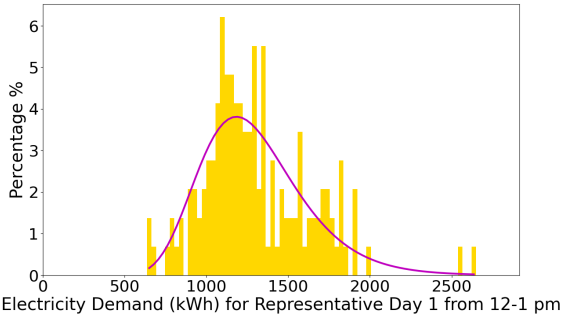

(a) The probability distribution function of electricity demand is an f distribution.

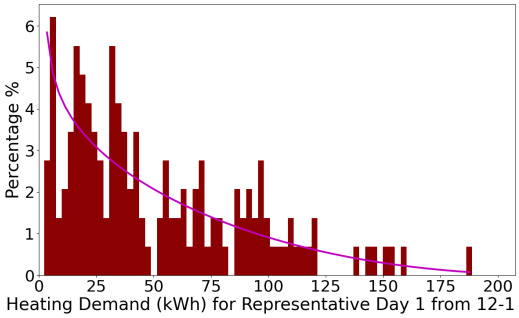

(b) The probability distribution function of heating demand is a beta distribution.

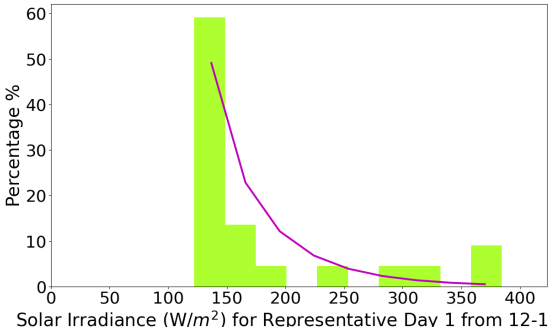

(c) The probability distribution function of solar irradiance is a chi distribution.

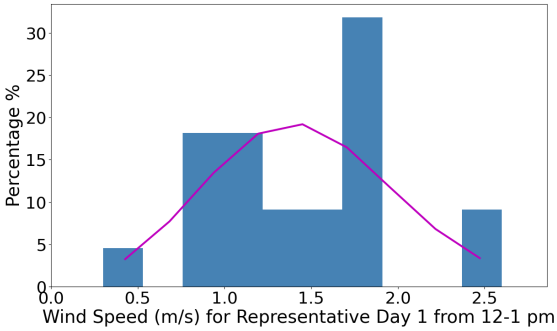

(d) The probability distribution function of wind speed is a weibull distribution.

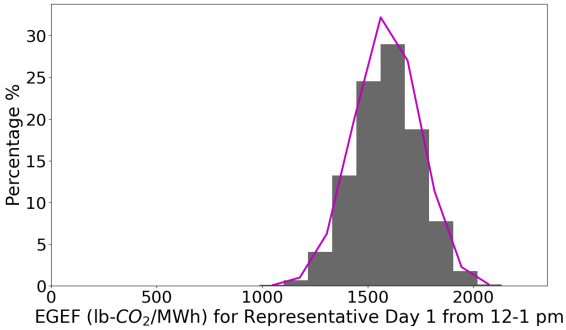

(e) The probability distribution function of electricity generation emission factor (EGEF) is a beta distribution.

Figure 7: The probability distribution function of electricity demand (a), heating demand (b), solar irradiance (c), wind speed (d), and electricity generation emission factor (EGEF) (e) for the Representative Day 1 from 12–1 pm.

hour for the uncertain input. For example, the T value for solar irradiance and wind speed is 22, the number of years (1998–2019) of historical data. The transition matrix represents transition probability for all intervals in each hour. For example, $P_{1,1}$ for solar irradiance represents the probability that solar irradiance is from 125–130.5 (W/m^2) (interval 1 in the current hour) at 12 pm and will transition to 125–129.5 (W/m^2) at 1 pm (interval 1 in the next hour). The transition matrix ($M_{d,h}$) is formed for each hour of the day (Equation 13):

$$M_{d,h} = \begin{pmatrix} P_{1,1} & P_{1,2} & \cdots & P_{1,50} \\ P_{2,1} & P_{2,2} & \cdots & P_{2,50} \\ \vdots & \vdots & \ddots & \vdots \\ P_{50,1} & P_{50,2} & \cdots & P_{50,50} \end{pmatrix} \tag{13}$$

3. A random number from the PDF of the uncertain input is generated to select an interval in the next hour (j').
4. Another random number (u) is generated from a uniform distribution from 0 to 1 ($0 \leq u \leq 1$).
5. The probability of transition from the current interval (i') to the next selected interval (j') in step 3 is compared to the random number from 0 to 1 (i.e., $P_{i',j'}$ is compared to u). If $P_{i',j'}$ is higher than u, the transition is accepted. If not, steps 3–5 are iterated until a transition is accepted.

This process is performed for each hour of the representative days and iterated for each representative day until the condition to end the iteration is met. Using the MCMC method, 10,000 yearly scenarios are generated for the variable energy demands, solar irradiance, wind speed, and annualized EGEF. These scenarios are used in the DES mathematical formulation to find the optimum operation planning of the DES and minimize the operating cost and CO_2 emissions.

3. Results and Discussion

In this section, a comprehensive comparison of the MILP solver as a classical method versus the NSGA-II algorithm as a metaheuristic method is presented on the optimization problem formed in Subsection 2.2. We evaluate how their performances and characteristics vary with respect to the minimized cost and CO_2 emissions, planned operation, computation time, initial knowledge needed to run the simulation, accessibility (open-source/free status), and satisfaction of constraints.

3.1. Cost and CO_2 emissions trade-off

Figure 8 shows the operating cost and CO_2 emissions using the MILP solver and NSGA-II algorithm. The results from the MILP solver are almost identical to the results from the NSGA-II algorithm, which shows for both methods, the same operating cost and CO_2 emissions are quantified. The cost and CO_2 emissions trade-off are shown by a Pareto front of 11 points for each scenario, where each point is at least better in one objective (cost or emissions) compared to other points, and no point is superior in both cost and emissions. For each scenario, these Pareto points represent a different combination of operation planning of energy components, which are natural gas consumption of boilers, natural gas consumption of the CHP system, electricity stored in batteries, and electricity purchased from the grid. The optimization is performed considering 10,000 stochastic scenarios and one deterministic scenario over a year, which all are shown in Figure 8.

The Pareto front of each scenario is linear (Figure 8). As electricity price is assumed constant at the UU throughout the year, the same control policy of renewables and batteries is applied to all 11 Pareto points. In the control policy, electricity generated by renewables is used to satisfy the electricity demands of buildings, and the remaining electricity from renewables is stored in batteries (more details in Subsection 2.1). Thus, decisions that can impact the cost-emissions trade-off of 11 points in the Pareto front are the amount of natural gas consumption to operate the CHP system and boilers. To satisfy the electricity and hot water demands of buildings, the energy constraints in the linear Equations 7 and 8 must be met. Therefore, the CHP system, boilers, and the grid are linearly related in each hour, resulting in a linear Pareto front for each scenario.

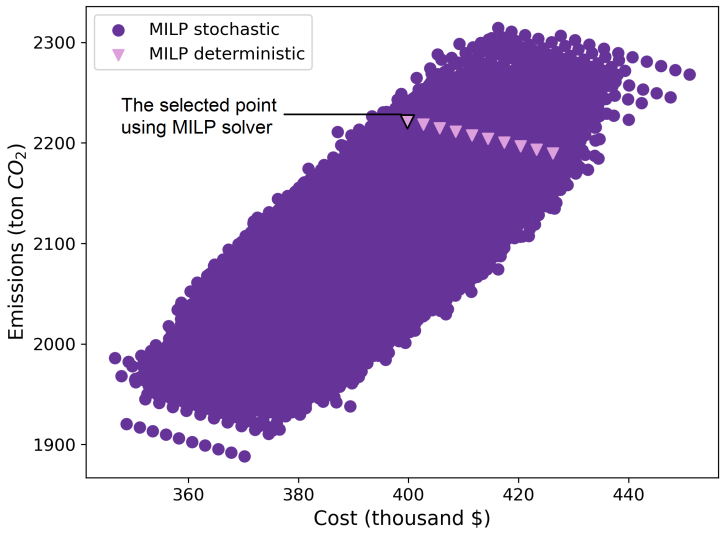

a. MILP solver

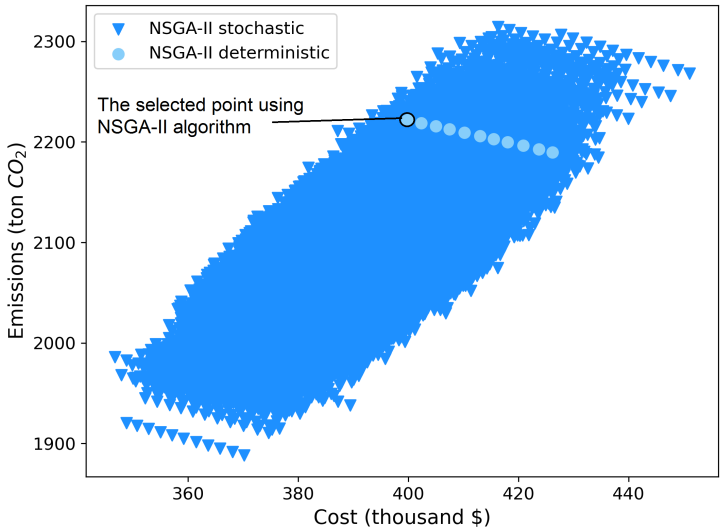

b. NSGA-II algorithm

Figure 8: Cost and CO_2 emissions trade-off while using the MILP solver and NSGA-II algorithm. Each point represents the operation planning of energy components throughout the year. Cost and emissions are almost identical when using the MILP solver vs. NSGA-II algorithm.

These two methods similarly plan the operation of energy components with slight differences in their solutions. As MILP solver and NSGA-II algorithm found similar solutions (Figure 8), it is difficult to distinguish their differences in the operating cost and CO_2 emissions. To check the difference in the solution of the two methods quantitatively, two points are selected as an example from the optimum deterministic scenario (Figure 8). The operating cost and CO_2 emissions of the selected points throughout the year are \$399,773 and 2,221,967 (kg CO_2) using the MILP method and \$399,819 and 2,221,910 (kg CO_2) using the NSGA-II algorithm. Comparing the two methods, the difference in the total operating cost and CO_2 emissions is less than 0.02% for the selected points throughout the year, demonstrating a negligible difference in the calculated cost and CO_2 emissions of the two methods.

3.2. Operation planning of the DES

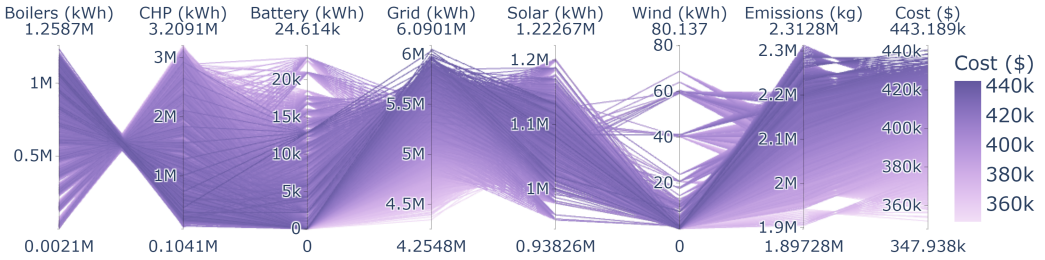

a. MILP solver

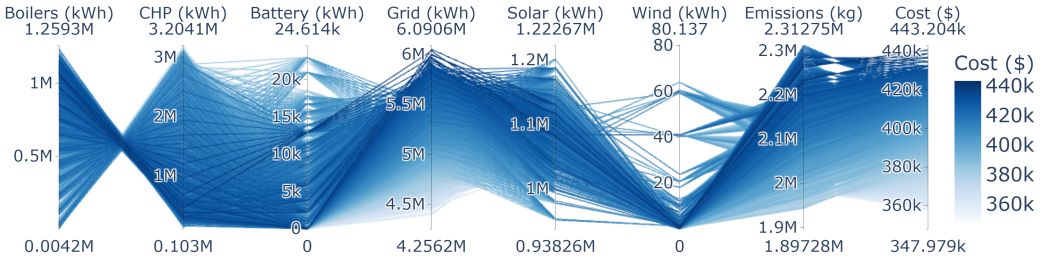

b. NSGA-II algorithm

Figure 9: Comparison of parallel coordinates plot showing the variation in the optimum operation planning of energy components in a year to minimize the operating cost and CO_2 emissions for the 10,000 generated scenarios. These variations are almost identical when using the MILP solver versus the NSGA-II algorithm.

The range of optimum decisions in operating the DES to minimize cost and CO_2 emissions in a year for the 10,000 stochastic scenarios are evaluated by performing the MILP solver (Figure 9a) and the NSGA-II algorithm (Figure 9b). These figures show the range of decision space for the operation planning of energy components, which are the natural gas consumption of boilers, natural gas consumption of the CHP system, electricity stored in batteries, electricity purchased from the grid, electricity generated by the solar PV system, electricity generated by the wind turbines, and their associated cost and CO_2 emissions. In the figure, each line represents a different combination of operation planning of energy components for one scenario throughout the year. Visual inspection of these two figures shows the range of decisions for operating the CHP system, boilers, batteries, solar PV, and wind turbines is almost identical using either the MILP solver or NSGA-II algorithm. This similarity results in comparable ranges of operating cost (from \$348.0k to \$443.2k for both methods) and CO_2 emissions (from 1,897, to 2,312 metric-ton CO_2 for both methods) throughout the year. The figures also show that in scenarios where more electricity is purchased from the grid, the operating cost is high (dark lines) compared to the other scenarios. This trend is because, in our case study, the operating cost of electricity purchased from the grid (0.069\$/kWh) is more expensive relative to the variable operating cost of electricity generated from the renewables (0\$/kWh) and the CHP system

Table 3: Statistical information of operation planning of energy components when the **MILP** solver is used for three points in the Pareto front."min cost" is when the cost is minimum, "med cost" is when the cost is median, and "max cost" is when the cost is maximum among all the points in the Pareto front, when "cons" is consumption, "gen" is generation, and "elect" is electricity.

	Mean min cost	STD dev min cost	CV % min cost	Mean med cost	STD dev med cost	CV % med cost	Mean max cost	STD dev max cost	CV % max cost
Boilers gas cons (MWh)	28.69	11.64	40.56	503.95	20.54	4.08	1098.03	41.81	3.81
CHP gas cons (MWh)	2924.12	79.21	2.71	1781.66	59.43	3.34	353.6	75.51	21.35
Battery stored elect (MWh)	2.65	3.85	145.36	2.65	3.85	145.36	2.65	3.85	145.36
Grid purchase (MWh)	4815.65	146.29	3.04	5143.53	145.61	2.83	5553.39	146.33	2.63
Solar gen elect (MWh)	1088.66	33.8	3.1	1088.66	33.8	3.1	1088.66	33.8	3.1
Wind gen elect (kWh)	1.61	5.58	346.84	1.61	5.58	346.84	1.61	5.58	346.84
CO_2 emissions (metric ton)	2126.94	50.23	2.36	2112.03	50.28	2.38	2093.39	50.37	2.41
Cost (thousand $)	384.56	9.81	2.55	394.41	9.82	2.49	406.72	9.85	2.42

(0.064$/kWh). It should be noted that this comparison is only regarding the operating cost, as this study is focused on the operation planning of the DES. Hence, the capital cost to buy the renewables and the CHP system is not included in the optimization framework to minimize the cost (Equation 3), and we assumed the renewables and the CHP system are already purchased.

3.3. Statistical information of operation planning

To quantify the variabilities of operating the energy components and their associated cost and CO_2 emissions, we collected their mean, standard deviation (STD), and coefficient of variation (CV) for the 10,000 generated scenarios for the MILP solver (Table 3) and the NSGA-II algorithm (Table 4). CV is the STD divided by the mean of each data series. As the CV is unitless, it is a suitable measure to compare the variabilities among the operation planning of energy components and their associated cost/CO_2 emissions, where their units are different (e.g., kWh, $, and kg CO_2). Three Pareto points among the 11 points in the Pareto front are shown in the tables representing the "min cost", "med cost", and "max cost". The "min cost" is when the cost is minimum and the emissions are maximum; the "med cost" is when the cost and emissions are median; and the "max cost" is when the cost is maximum, and the emissions are minimum among all Pareto points. Similar to Prabatha et al. (2021)'s study, we can see in Tables 3 and 4 that considering the uncertainties in energy demands, solar irradiance, wind speed, and annualized electricity-related emissions results in variations in operation planning of the DES and consequently, variation in the calculated cost and CO_2 emissions. These two tables show that the operation planning of the DES, calculated operating cost, and calculated operating CO_2 emissions are very similar for the Pareto points using the MILP solver vs. the NSGA-II algorithm.

From "Mean min cost" to "Mean max cost" in Tables 3 and 4, the mean of the electricity purchased from the grid increases, and the natural gas consumption of the CHP system decreases. This trend conveys that operating the CHP system more often results in purchasing less electricity from the grid. In our case study, purchasing less electricity from the grid reduces the calculated operating cost and increases the quantified CO_2 emissions at the UU. This is because the EGEF at the UU is weighted down to account for the UU clean electricity purchase (more details in Subsection 2.1). Therefore, using the lower EGEF at the UU (Table A.1) compared to the standard EGEF in Utah (U.S. EIA, 2019) decreases the emissions when purchasing more electricity from the grid compared to other scenarios.

Table 4: Statistical information of operation planning of energy components when the **NSGA-II** algorithm is used for three points in the Pareto front. "min cost" is when the cost is minimum, "med cost" is when the cost is median, and "max cost" is when the cost is maximum among all the points in the Pareto front, when "cons" is consumption, "gen" is generation, and "elect" is electricity.

	Mean min cost	STD dev min cost	CV % min cost	Mean med cost	STD dev med cost	CV % med cost	Mean max cost	STD dev max cost	CV % max cost
Boilers gas cons (MWh)	30.78	11.63	37.77	560.93	24.2	4.31	998.17	38.93	3.9
CHP gas cons (MWh)	2919.09	79.12	2.71	1644.69	60.61	3.69	593.64	72.18	12.16
Battery stored elect (MWh)	2.65	3.85	145.36	2.65	3.85	145.36	2.65	3.85	145.36
Grid purchase (MWh)	4817.09	146.29	3.04	5182.85	145.53	2.81	5484.5	146.06	2.66
Solar gen elect (MWh)	1088.66	33.8	3.1	1088.66	33.8	3.1	1088.66	33.8	3.1
Wind gen elect (kWh)	1.61	5.58	346.84	1.61	5.58	346.84	1.61	5.58	346.84
CO_2 emissions (metric ton)	2126.88	50.23	2.36	2110.27	50.3	2.38	2096.56	50.37	2.4
Cost (thousand $)	384.6	9.81	2.55	395.59	9.82	2.48	404.65	9.84	2.43

The mean, STD, and CV of the electricity stored by batteries, electricity generated by the solar PV system, and wind turbines remain constant for both methods and all Pareto points (Tables 3 and 4). This trend is because the control policy of batteries and renewable resources are the same for all Pareto points (more details in Subsection 2.1). Therefore, the Pareto points are similar in the amount of electricity generated from renewables and electricity stored in batteries in each time step.

Both methods demonstrate that the maximum CV is for electricity generated by wind turbines (346.8%), and the second-largest CV is for the stored energy by batteries (145.4%) compared to the CVs of the electricity generated by the solar PV, electricity purchased from the grid, natural gas consumption of boilers and the CHP system (Tables 3 and 4). This trend indicates that the electricity generated by wind turbines and electricity stored in batteries are associated with the larger spread and variability of operation compared to operating the solar PV, boilers, and the CHP system. One reason for the high CV of electricity from wind turbines is that variabilities in wind speed are directly used in the uncertainty analysis of this study (Equation 10), where the electricity from wind turbines is related to the cube of wind speed. Moreover, considerable variabilities (CV of 52%) are present in wind speed representing the changes in wind speed values in 2019 in Salt Lake City. Variabilities in solar irradiance are also significant (CV of 135%) and directly used in the uncertainty analysis. However, these solar irradiance variabilities do not result in substantial variabilities in the electricity from solar PV as its electricity generation is limited by the power density of the PV modules.

The CV of operating cost and CO_2 emissions is from 2.36% to 2.55% when the MILP solver and NSGA-II algorithm are used for all Pareto points. The difference of calculated cost and CO_2 emissions between these two methods will not affect the early-stage decisions by the DES operators as greater uncertainties are present in this study. For instance, uncertainties are present in the electricity generated by the CHP system due to the changes in the efficiency of the CHP system by the load (i.e., partial load efficiency) (more discussion on the limitations in Section 4). These low CV values of cost and CO_2 emissions also show that although the variabilities in the electricity generated by the wind turbines (346.8%) and electricity stored in batteries (145.4%) are significant, the variability of calculated operating cost and CO_2 emissions is negligible and limited to 2.6% for both methods and all Pareto points.

3.4. Practical comparison of MILP and NSGA-II

Table 5 shows a comparison between the MILP solver and NSGA-II algorithm with respect to the computation time, type of optimization problem, implementation, accessibility (open-source/free status), parallel

Table 5: Comparing the performance characteristics of MILP solver vs. NSGA-II algorithm.

Items	MILP solver	NSGA-II algorithm	Preferred method
Computation time	24 seconds to optimize 1 day	60 seconds to optimize 1 day	MILP
Optimization problem	Originally used for single objective (e.g., needs ϵ-constraint for multi-objective), targets linear problems	Only works for multi-objective, targets both linear and non-linear problems	Depends on the problem
Implementation	Only needs the population size	Needs several initial parameters (Table 2)	MILP
Accessibility (Open-source/Free)	No, in general, some are free for academics (e.g., CPLEX) a few are free and open-source (e.g., GLPK)	Yes, several Python packages are available (e.g., Pymoo Blank and Deb (2020))	NSGA-II
Parallel computing	Yes, as an option in some software	Yes, easy implementation in some Python packages	Both
Satisfaction of constraints	Yes, gives an error for constraints violation	Yes (depends on the initial parameters), doesn't give an error for constraints violation	MILP

computation, and satisfaction of constraints.

Computation time: Computation time is the timespan required to optimize the operation planning of one representative day and generate its associated operating cost and CO_2 emissions. In this study, the computation time of performing the multi-objective optimization is 24 seconds using the MILP solver and 60 seconds using the NSGA-II algorithm for each representative day. The MILP solver is preferred to the NSGA-II algorithm regarding the computation time.

Optimization problem: To solve an optimization problem, a user should indicate if the problem is single-objective, multi-objective, linear, and/or non-linear. A MILP solver only solves linear and single-objective problems. With the help of methods such as weighted-sum or ϵ-constraint, a multi-objective problem can be solved by a MILP solver as well. The NSGA-II algorithm can solve multi-objective, linear, and non-linear problems. In this study, we implemented the ϵ-constraint method to solve the multi-objective optimization problem using a MILP solver, and no additional method was needed to implement the NSGA-II algorithm.

Implementation: Implementation represents the initial parameters necessary to perform the optimization. In the implementation of the MILP solver, the only initial parameter to set is the population size (Table 2), which represents the number of points in the Pareto front. However, in the implementation of the NSGA-II method, we should tune the population size, crossover probability, crossover distribution index, mutation probability, mutation distribution index, and the number of iterations (Table 2) before performing the multi-objective optimization. These parameters are effective in achieving the near-optimum solution with satisfied constraints in the NSGA-II algorithm. Tuning and changing these initial parameters in the NSGA-II algorithm also requires some knowledge about the algorithm. Therefore, implementing the MILP solver is easier compared to the NSGA-II.

Accessibility (Open-source/Free): A framework is accessible by being open-source and free when a user can execute the code behind it at no cost and have access to its source code for customized purposes. In this study, the GLPK solver performs the optimization using the MILP solver, and Platypus (D. Hadka, 2019) performs the optimization using the NSGA-II algorithm, where both of them are open-source and free. Several Python packages such as Pymoo (Blank and Deb, 2020), DEAP (Fortin et al., 2012), and Platypus (D. Hadka, 2019) are available to implement the NSGA-II algorithm in an open-source/free framework. Although some of the leading MILP solvers (e.g., CPLEX and Gurobi) are free for academics and some (e.g., GLPK and COIN-OR LP) are free for all users (for more info, please read Gearhart et al. (2013)), an open-source and free framework is not a default feature of MILP solvers. Thus, more options are available to implement the NSGA-II algorithm in an open-source and free framework compared to the MILP solver.

Parallel computation: Parallel computation uses the processing unit's power (e.g., CPU cores) to execute an independent block of programs in parallel when executing a simulation with heavy computation. Tools are available to perform parallel computing for both MILP solver and NSGA-II algorithm, but an open-source tool that implements parallel computing is only available for the NSGA-II algorithm. Parallel computing is an option in some proprietary MILP solvers (e.g., CPLEX, GAMS, and Gurobi). To perform the NSGA-II algorithm, parallel computing is available in Python packages such as Platypus (D. Hadka, 2019). For other packages, a user can use parallel platforms (Burtscher and Rabeti, 2013) and parallel debuggers (Taheri et al., 2017, 2019) to implement the problem, which requires programming expertise. In this study, parallel computing has been used in the Platypus (D. Hadka, 2019) to perform the NSGA-II algorithm and not used in the MILP solver.

Satisfaction of constraints: Satisfaction of constraints in this paper refers to the way that optimization methods check if constraints are satisfied or not. To check the satisfaction of constraints, we investigate whether an optimization method has selected an operating point that constraints (e.g., the electricity demand in each hour) are satisfied and how the optimization method would behave if constraints are not satisfied. In this study, by tuning the initial parameters with trial and error (Table 2), both methods satisfy the constraints. However, the satisfaction of constraints is different between the MILP solver and the NSGA-II algorithm in general. The MILP solver must satisfy the constraints; otherwise, it gives an error. This error can help improve and debug a user's code. However, when the NSGA-II algorithm is performed, the constraints satisfaction depends on the convergence of solutions, and it is the user's responsibility to check if constraints are satisfied or not. Therefore, the satisfaction of constraints using the MILP solver is more straightforward than the NSGA-II algorithm.

In summary, the results of this section are used to compare the MILP solver and NSGA-II algorithm regarding the calculated operating cost and CO_2 emissions, the operation of energy components, computation time, implementation, accessibility (open-source/free status), and satisfaction of constraints. Both methods present similar results for the operation planning, operating cost, and operating CO_2 emissions. However, some characteristics of the MILP solver and NSGA-II algorithm are different. More open-source/free tools are available to implement the NSGA-II algorithm compared to the MILP solver. The MILP solver performs the optimization 2.5 times faster than the NSGA-II algorithm. Implementing the MILP solver is easier as it needs fewer initial parameters than the NSGA-II algorithm. The satisfaction of constraints in the MILP solver is also more straightforward to be checked compared to the NSGA-II algorithm. The optimization code is presented as an open-source framework (Z. Ghaemi, A.D. Smith, 2021), which can help future researchers select the suitable optimization method related to their case study.

4. Limitations and future work

In this paper, a multi-objective optimization to minimize cost and CO_2 emissions was performed on a multi-use DES considering uncertainties in energy demands, solar irradiance, wind speed, and annualized electricity-related emissions. Performing this optimization involved the following limitations:

1. The uncertainties were generated from the actual values of uncertain inputs in this study. The actual values of uncertain inputs consist of electricity demand, hot water demand, wind speed, solar irradiance, and annualized electricity-related emissions. However, in a real-world case study, the actual values of uncertain inputs are unknown by the DES operators. These values can be predicted by using physics-based models, statistical models, machine learning algorithms, and/or a combination of all methods. The prediction methods are not included in this study as we focused on an early stage operation planning of the DES, where the goal is to evaluate the variabilities in the final cost and CO_2 emissions.

   The DES operators can use historical data in this study's framework to optimize the operation planning for case studies that their energy demands and weather parameters are not extremely different from year to year. If the historical data is extremely different over the years, the operation planning of this study is not valid by using historical data.

   To quantitatively evaluate the effects of the changes in meteorological parameters and energy demands, we used the meteorological data of the case study in 2018 and changed the energy demands of the case study in 2019 by a specific percentage (p). This comparison showed that the operating cost and CO_2 emissions differed by approximately the same percentage (p) compared to the case study in 2019.

For example, if the energy demands are different by 8% from year to year, then the operating cost and emissions are also different by ≈8%. DES planners and operators who make decisions based on historical energy demands should be aware of the year-to-year variation of demands and the potential impact of this variation on the optimality of decisions related to operation planning.

2. Representative days were used instead of the actual days in this study by using the historical data of energy demands. The optimization was performed on one deterministic scenario to compare the computation time and results between using representative days versus the actual days. When using representative days and the actual days, the operating cost and CO_2 emissions were different by 9%. The computation time of optimization under uncertainties was around three days (70 hours) on a laptop (16 GB of memory and Intel Core-i7 at 2.20GHz) using representative days when 10,000 stochastic scenarios were generated. The computation time to optimize the same problem considering 10,000 stochastic scenarios for actual days was estimated at around three months and ten days (2,389 computation hours = (70 computation hours)/(11 representative days)×(365 actual days)) on the same laptop. Hence, the computation time using the representative days was reasonably short to evaluate the effects of variabilities in energy demands, solar irradiance, wind speed, and annualized electricity-related emissions on the calculated operation cost and CO_2 emissions of the DES.

3. Energy component characteristics were assumed constant due to the early-stage analysis of the DES. However, the efficiencies of energy components change by their load, outside temperature, and the number of cycles they undergo. For instance, for a microturbine CHP system, the electrical efficiency was reduced by 15% when it was operated at 50% of its maximum capacity (Rosfjord et al., 2008). To capture the partial load behavior of the DES, we suggest that a user first performs the optimization using the constant characteristic of energy components. Then, based on the suggested operation planning, users can apply the effects of changes in the characteristic of energy components and evaluate the magnitude of changes in the operating cost and emissions. Another suggested method is to take the performance and efficiency curves from their selected manufacturers of energy components and format them as an input to generate more realistic results than using constant efficiency values. Using the second method causes non-linearity in the optimization, which increases the computation time of providing an optimum solution using the NSGA-II algorithm. The efficiency curves in the second method cannot be included in the optimization problem by the MILP solver as they can only optimize linear problems.

4. Energy prices were assumed constant due to the electricity and natural gas purchasing policies of the UU. However, commercial buildings do not get charged the same price for their electricity demands and may purchase electricity at different utility rate schedules. This means that the price of electricity varies over a day, month, and/or season depending on the time of use rate and electricity demand charges stated in their utility contract. In this study, the electricity price is assumed constant throughout the year. The constant electricity price is levelized at the UU by dividing the total purchased cost of electricity ($) by the total electricity purchased from the grid over a year (kWh). Thus, the rate schedule in our case study can be different from the rate schedule of typical commercial buildings. This can impact the operating policy of batteries and consequently affect the operation of energy components and their calculated cost and CO_2 emissions in case studies with different rate schedules. To evaluate different rate schedules in the DES, we suggest taking the rate schedule of a group of commercial buildings and formatting it as an input to consider variable energy prices. Using this method increases the computation time of providing an optimum solution.

5. The scenario generation of energy demands, solar irradiance, wind speed, and electricity-related emissions in each hour depends only on the value of the uncertain input in the previous hour. This is because we implemented the first-order Markov chain in the scenario generation. We used this method as the first-order Markov chain has been widely performed to generate sequential scenarios of wind speed and solar irradiance (Mavromatidis et al., 2018a; Li et al., 2020). A user can change the method to a second-order Markov chain (e.g., Jeyakumar et al. (2021); Ayodele et al. (2019)) to consider the effects of the two previous hours on the values of uncertain inputs. The disadvantage of using a second-order Markov chain is the higher computation time compared to the first-order Markov chain.

6. The correlation of uncertain inputs (i.e., energy demands, solar irradiance, wind speed, and electricity-related emissions) were neglected when implementing the MCMC method. However, the solar irradiance is correlated with the energy demands of buildings. For example, when solar irradiance increases, the electricity demand increases and heating demand decreases (Wan et al., 2011). We neglected the correlations between the uncertain inputs as they would decrease the variabilities of operating cost and CO_2 emissions in the DES. By not considering the correlation of uncertain inputs, we over-estimated the variabilities in the operation planning of the DES, which is already limited to 2.6%. Therefore, we neglected the correlation of uncertain inputs in this study.

In future work, including the next day predictions in energy demands, solar irradiance, and wind speed to the framework of multi-use multi-objective optimization of the DES under uncertainties can help the operators of the DES with practical decision-making. Another potential for future work is the inclusion of mixed-integer non-linear programming solvers in the framework to enable optimization of non-linear problems using a classical method. This enables the inclusion of partial load efficiencies of energy components in the optimization framework using the classical method. Hence, including the mixed-integer non-linear programming solver expands the applicability of the framework to both linear and non-linear problems using classical and metaheuristic algorithms.

5. Conclusions

The key contributions of this work are (1) performing a multi-objective optimization to minimize the operating cost and CO_2 emissions of a multi-use district energy system (DES) given the uncertainties; (2) comparing two widely used methods, a mixed-integer linear programming (MILP) solver and non-dominated sorting genetic algorithm (NSGA-II); and (3) presenting an open-source framework (Z. Ghaemi, A.D. Smith, 2021) to perform a multi-objective optimization of operation planning of the DES under uncertainties.

The MILP solver and NSGA-II algorithm presented the results of the operations of energy components, operating cost, and operating CO_2 emissions, similarly. However, some characteristics of the MILP solver and the NSGA-II algorithm are different. More open-source/free tools are available to implement the NSGA-II algorithm compared to the MILP solver. The MILP solver performs the optimization 2.5 times faster than the NSGA-II algorithm. Implementing the MILP solver is easier as it needs fewer initial parameters than the NSGA-II algorithm. It is more straightforward to check the satisfaction of constraints in the MILP solver compared to the NSGA-II algorithm.

The effects of uncertainties in energy demands, solar irradiance, wind speed, and annualized electricity-related emissions on the operating cost and CO_2 emissions are presented using the coefficient of variation (CV), the standard deviation divided by the mean of each data series. The variabilities are significant in the electricity generated by the wind turbine (346.8% of the mean of the electricity generated from wind turbines) and the electricity stored in batteries (145.4% of the mean of electricity stored in batteries). The CV of operating cost and CO_2 emissions is from 2.3% to 2.6% when using the MILP solver and NSGA-II algorithm. Thus, the results of this study show that although variabilities in renewables are considerable, the variability of calculated operating cost and CO_2 emissions is negligible and limited to 2.6% for both methods.

This study presents a novel open-source framework by modeling a mixed-used multi-objective DES that considers uncertainties in weather parameters, energy demands, and annualized electricity-related emissions.

Funding

This research did not receive any specific grant from funding agencies in the public, commercial, or not-for-profit sectors.

CRediT authorship contribution statement

Zahra Ghaemi: Conceptualization, Data curation, Formal analysis, Investigation, Methodology, Software, Visualization, Writing - original draft, and Writing - review & editing. **Thomas T. D. Tran**: Conceptualization, Writing - review & editing. **Amanda D. Smith**: Conceptualization, Methodology, Project administration, Supervision, and Writing - review & editing.

Acknowledgements

We appreciate the assistance and support by the UU Department of Facilities Management by providing the energy demands data, the insights from Dr. Keunhan Park, Dr. Mathieu Francoeur, and Dr. Sameer Rao in the conceptualization of this paper, and the help of Dr. Amanda Funai and Dr. Saeed Taheri in reviewing and editing the writing of this paper.

References

M. N. Ab Wahab, S. Nefti-Meziani, A. Atyabi, A comparative review on mobile robot path planning: Classical or meta-heuristic methods?, Annual Reviews in Control 50 (2020) 233–252.

M. Abbaspour, M. Satkin, B. Mohammadi-Ivatloo, F. H. Lotfi, Y. Noorollahi, Optimal operation scheduling of wind power integrated with compressed air energy storage (CAES), Renewable Energy 51 (2013) 53–59.

M. Abdel-Basset, L. Abdel-Fatah, A. K. Sangaiah, Metaheuristic algorithms: A comprehensive review, Computational intelligence for multimedia big data on the cloud with engineering applications (2018) 185–231.

A. Alarcon-Rodriguez, G. Ault, S. Galloway, Multi-objective planning of distributed energy resources: A review of the state-of-the-art, Renewable and Sustainable Energy Reviews 14 (5) (2010) 1353–1366.

A. Alhamwi, W. Medjroubi, T. Vogt, C. Agert, Development of a GIS-based platform for the allocation and optimisation of distributed storage in urban energy systems, Applied Energy 251 (2019) 113360.

J. Allegrini, K. Orehounig, G. Mavromatidis, F. Ruesch, V. Dorer, R. Evins, A review of modelling approaches and tools for the simulation of district-scale energy systems, Renewable and Sustainable Energy Reviews 52 (2015) 1391–1404.

O. O. Amusat, P. R. Shearing, E. S. Fraga, Optimal design of hybrid energy systems incorporating stochastic renewable resources fluctuations, Journal of Energy Storage 15 (2018) 379–399.

A. K. Arya, A comparison of the MOGA and NSGA-II optimization techniques to reduce the cost of a biomass supply network, Materials Today: Proceedings .

T. Ayodele, A. Ogunjuyigbe, R. Olarewaju, J. Munda, Comparative assessment of wind speed predictive capability of first-and second-order Markov chain at different time horizons for wind power application, Energy Engineering 116 (3) (2019) 54–80.

M. A. Bagherian, K. Mehranzamir, A. B. Pour, S. Rezania, E. Taghavi, H. Nabipour-Afrouzi, M. Dalvi-Esfahani, S. M. Alizadeh, Classification and Analysis of Optimization Techniques for Integrated Energy Systems Utilizing Renewable Energy Sources: A Review for CHP and CCHP Systems, Processes 9 (2) (2021) 339.

R. Banos, F. Manzano-Agugliaro, F. Montoya, C. Gil, A. Alcayde, J. Gómez, Optimization methods applied to renewable and sustainable energy: A review, Renewable and sustainable energy reviews 15 (4) (2011) 1753–1766.

M. Bastani, H. Damgacioglu, N. Celik, A δ-constraint multi-objective optimization framework for operation planning of smart grids, Sustainable Cities and Society 38 (2018) 21–30.

J. Blank, K. Deb, Pymoo: Multi-Objective Optimization in Python, IEEE Access 8 (2020) 89497–89509.

M. Bornapour, R.-A. Hooshmand, A. Khodabakhshian, M. Parastegari, Optimal stochastic scheduling of CHP-PEMFC, WT, PV units and hydrogen storage in reconfigurable micro grids considering reliability enhancement, Energy conversion and management 150 (2017) 725–741.

I. Boussaïd, J. Lepagnot, P. Siarry, A survey on optimization metaheuristics, Information sciences 237 (2013) 82–117.

M. Burtscher, H. Rabeti, A scalable heterogeneous parallelization framework for iterative local searches, in: 2013 IEEE 27th International Symposium on Parallel and Distributed Processing, IEEE, 1289–1298, 2013.

Y. Cao, H. A. Dhahad, N. Farouk, W.-F. Xia, H. N. Rad, A. Ghasemi, S. Kamranfar, M. M. Sani, A. A. Shayesteh, Multi-objective Bat Optimization for a Biomass Gasifier Integrated Energy System Based on 4E Analyses, Applied Thermal Engineering (2021) 117339.

M. Capone, E. Guelpa, V. Verda, Multi-objective optimization of district energy systems with demand response, Energy 227 (2021) 120472.

S. Collins, J. P. Deane, K. Poncelet, E. Panos, R. C. Pietzcker, E. Delarue, B. P. Ó. Gallachóir, Integrating short term variations of the power system into integrated energy system models: A methodological review, Renewable and Sustainable Energy Reviews 76 (2017) 839–856.

Courtney Tanner, Most of the University of Utah's electricity will now be fueled by renewable energy, https://www.sltrib.com/news/education/2020/02/11/university-utah-will-now/, accessed: 2021-03-15, 2020.

I. I. Cplex, V12. 1: User's Manual for CPLEX, International Business Machines Corporation 46 (53) (2009) 157.

D. Hadka, Platypus: Multiobjective Optimization in Python, https://platypus.readthedocs.io, 2019.

K. Darrow, R. Tidball, J. Wang, A. Hampson, Catalog of CHP technologies; 2015, US Environmental Protection Agency and the US Department of Energy https://www.epa.gov/sites/production/files/2015-07/documents/catalog_of_chp_technologies.pdf.

K. Deb, A. Pratap, S. Agarwal, T. Meyarivan, A fast and elitist multiobjective genetic algorithm: NSGA-II, IEEE transactions on evolutionary computation 6 (2).

A. Dini, A. Hassankashi, S. Pirouzi, M. Lehtonen, B. Arandian, A. A. Baziar, A flexible-reliable operation optimization model of the networked energy hubs with distributed generations, energy storage systems and demand response, Energy 239 (2022) 121923.

A. P. Dobos, PVWatts version 5 manual, 2014.

G. G. Dranka, P. Ferreira, A. I. F. Vaz, A review of co-optimization approaches for operational and planning problems in the energy sector, Applied Energy 304 (2021) 117703.

M. Q. Duong, B. T. M. Le Hong Lam, G. Q. H. Tu, N. H. Hieu, Combination of K-Mean clustering and elbow technique in mitigating losses of distribution network, GMSARN International (2019) 153–158.

E. Dupont, R. Koppelaar, H. Jeanmart, Global available wind energy with physical and energy return on investment constraints, Applied Energy 209 (2018) 322–338.

Energy Information Administration (EIA), Monthly energy review, https://www.eia.gov/totalenergy/data/monthly/pdf/mer.pdf, accessed: 06-06-2021, 2021.

S. Evans, P. Clausen, Modelling of turbulent wind flow using the embedded Markov chain method, Renewable Energy 81 (2015) 671–678.

S. Fazlollahi, S. L. Bungener, P. Mandel, G. Becker, F. Maréchal, Multi-objectives, multi-period optimization of district energy systems: I. Selection of typical operating periods, Computers & Chemical Engineering 65 (2014) 54–66.

S. Fazlollahi, P. Mandel, G. Becker, F. Maréchal, Methods for multi-objective investment and operating optimization of complex energy systems, Energy 45 (1) (2012) 12–22.

F.-A. Fortin, F.-M. De Rainville, M.-A. Gardner, M. Parizeau, C. Gagné, DEAP: Evolutionary Algorithms Made Easy, Journal of Machine Learning Research 13 (2012) 2171–2175.

P. Gagnon, R. Margolis, J. Melius, C. Phillips, R. Elmore, Rooftop solar photovoltaic technical potential in the U.S.. A detailed assessment, 2016.

J. L. Gearhart, K. L. Adair, R. J. Detry, J. D. Durfee, K. A. Jones, N. Martin, Comparison of open-source linear programming solvers, Sandia National Laboratories, SAND2013-8847 .

Z. Ghaemi, A. D. Smith, A review on the quantification of life cycle greenhouse gas emissions at urban scale, Journal of Cleaner Production 252 (2020) 119634.

Z. Ghaemi, A. D. Smith, Analyzing variability and decomposing electricity-generation emission factors for three US states, Sustainable Energy Technologies and Assessments 51 (2022) 101986, https://doi.org/10.31224/osf.io/kstgn.

Z. Ghaemi, T. T. Tran, A. D. Smith, Sizing Optimization of District Energy Systems Considering Meteorological, Demand, and Electricity Emission Factor Uncertainties, in: ASME International Mechanical Engineering Congress and Exposition, vol. 85635, American Society of Mechanical Engineers, V08AT08A002, https://doi.org/10.31224/osf.io/hcnd6, 2021.

M. Ghiasi, Detailed study, multi-objective optimization, and design of an AC-DC smart microgrid with hybrid renewable energy resources, Energy 169 (2019) 496–507.

F. Guo, Y. Li, Z. Xu, J. Qin, L. Long, Multi-objective optimization of multi-energy heating systems based on solar, natural gas, and air-energy, Sustainable Energy Technologies and Assessments 47 (2021) 101394.

M. P. HA, P. D. Huy, V. K. Ramachandaramurthy, A review of the optimal allocation of distributed generation: Objectives, constraints, methods, and algorithms, Renewable and Sustainable Energy Reviews 75 (2017) 293–312.

W. E. Hart, C. D. Laird, J.-P. Watson, D. L. Woodruff, G. A. Hackebeil, B. L. Nicholson, J. D. Siirola, et al., Pyomo-optimization modeling in python, vol. 67, Springer, 2017.

W. E. Hart, J.-P. Watson, D. L. Woodruff, Pyomo: modeling and solving mathematical programs in Python, Mathematical Programming Computation 3 (3).

W. F. Holmgren, R. W. Andrews, A. T. Lorenzo, J. S. Stein, PVLIB python 2015, in: 2015 ieee 42nd photovoltaic specialist conference (pvsc), IEEE, 1–5, 2015.

W. F. Holmgren, C. W. Hansen, M. A. Mikofski, pvlib python: A python package for modeling solar energy systems, Journal of Open Source Software 3 (29) (2018) 884.

Z. Huang, Z. Xie, C. Zhang, S. H. Chan, J. Milewski, Y. Xie, Y. Yang, X. Hu, Modeling and multi-objective optimization of a stand-alone PV-hydrogen-retired EV battery hybrid energy system, Energy conversion and management 181 (2019) 80–92.

S. Ikeda, R. Ooka, Metaheuristic optimization methods for a comprehensive operating schedule of battery, thermal energy storage, and heat source in a building energy system, Applied energy 151 (2015) 192–205.

S. Islam, S. Ponnambalam, H. L. Lam, Review on life cycle inventory: methods, examples and applications, Journal of cleaner production 136 (2016) 266–278.

P. Jeyakumar, N. Kolambage, N. Geeganage, G. Amarasinghe, S. K. Abeygunawardane, Short-term Wind Power Forecasting Using a Markov Model, in: 2021 3rd International Conference on Electrical Engineering (EECon), IEEE, 19–24, 2021.

R. Jing, M. Wang, Z. Zhang, J. Liu, H. Liang, C. Meng, N. Shah, N. Li, Y. Zhao, Comparative study of posteriori decision-making methods when designing building integrated energy systems with multi-objectives, Energy and Buildings 194 (2019) 123–139.

M. A. Jirdehi, V. S. Tabar, R. Hemmati, P. Siano, Multi objective stochastic microgrid scheduling incorporating dynamic voltage restorer, International Journal of Electrical Power & Energy Systems 93 (2017) 316–327.

M. Karmellos, P. Georgiou, G. Mavrotas, A comparison of methods for the optimal design of distributed energy systems under uncertainty, Energy 178 (2019) 318–333.

R. Khezri, A. Mahmoudi, Review on the state-of-the-art multi-objective optimisation of hybrid standalone/grid-connected energy systems, IET Generation, Transmission & Distribution 14 (20) (2020) 4285–4300.

C. Klemm, P. Vennemann, Modeling and optimization of multi-energy systems in mixed-use districts: A review of existing methods and approaches, Renewable and Sustainable Energy Reviews 135 (2021) 110206.

C. W. Kurnik, G. Simons, S. Barsun, Chapter 23: Combined Heat and Power Evaluation Protocol. The Uniform Methods Project: Methods for Determining Energy Efficiency Savings for Specific Measures URL https://www.osti.gov/biblio/1406987.

G. Legorburu, A. D. Smith, Incorporating observed data into early design energy models for life cycle cost and carbon emissions analysis of campus buildings, Energy and Buildings 224 (2020) 110279.

J. Li, J. Zhou, B. Chen, Review of wind power scenario generation methods for optimal operation of renewable energy systems, Applied Energy 280 (2020) 115992.

Z. Li, C. Wang, B. Li, J. Wang, P. Zhao, W. Zhu, M. Yang, Y. Ding, Probability-interval-based optimal planning of integrated energy system with uncertain wind power, IEEE Transactions on Industry Applications 56 (1) (2019) 4–13.

G. Limpens, S. Moret, H. Jeanmart, F. Maréchal, EnergyScope TD: A novel open-source model for regional energy systems, Applied Energy 255 (2019) 113729.

R. Mafakheri, P. Sheikhahmadi, S. Bahramara, A two-level model for the participation of microgrids in energy and reserve markets using hybrid stochastic-IGDT approach, International Journal of Electrical Power & Energy Systems 119 (2020) 105977.

M. Mahmoud, M. Ramadan, S. Naher, K. Pullen, A. Baroutaji, A.-G. Olabi, Recent advances in district energy systems: A review, Thermal Science and Engineering Progress 20 (2020) 100678.

D. Marutho, S. H. Handaka, E. Wijaya, et al., The determination of cluster number at k-mean using elbow method and purity evaluation on headline news, in: 2018 International Seminar on Application for Technology of Information and Communication, IEEE, 533–538, 2018.

G. Mavromatidis, K. Orehounig, J. Carmeliet, Design of distributed energy systems under uncertainty: A two-stage stochastic programming approach, Applied energy 222 (2018c) 932–950.

G. Mavromatidis, K. Orehounig, J. Carmeliet, A review of uncertainty characterisation approaches for the optimal design of distributed energy systems, Renewable and Sustainable Energy Reviews 88 (2018a) 258–277.

G. Mavromatidis, K. Orehounig, J. Carmeliet, Uncertainty and global sensitivity analysis for the optimal design of distributed energy systems, Applied Energy 214 (2018b) 219–238.

A. A. Moghaddam, A. Seifi, T. Niknam, Multi-operation management of a typical micro-grids using Particle Swarm Optimization: A comparative study, Renewable and Sustainable Energy Reviews 16 (2) (2012) 1268–1281.

S. Nojavan, M. Majidi, A. Najafi-Ghalelou, M. Ghahramani, K. Zare, A cost-emission model for fuel cell/PV/battery hybrid energy system in the presence of demand response program: ε-constraint method and fuzzy satisfying approach, Energy Conversion and Management 138 (2017b) 383–392.

S. Nojavan, K. Zare, B. Mohammadi-Ivatloo, Optimal stochastic energy management of retailer based on selling price determination under smart grid environment in the presence of demand response program, Applied energy 187 (2017a) 449–464.

NREL, Distributed generation renewable energy estimate of costs Accessed: 2021-07-20.

NREL, Rooftop Solar Photovoltaic Technical Potential in the United States: A Detailed Assessment Accessed: 2021-08-25.

Parker industrial boiler, Up to 6,800,000 BTU Standard Atmospheric W/ Honeywell Flame Safeguard Manual, https://www.parkerboiler.com/download/up-to-6800000-btu-standard-atmospheric-w-honeywell-flame-safeguard-manual/, accessed: 2021-10-28, 2021.

S. Pfenninger, J. DeCarolis, L. Hirth, S. Quoilin, I. Staffell, The importance of open data and software: Is energy research lagging behind?, Energy Policy 101 (2017) 211–215.

B. Pickering, S. Ikeda, R. Choudhary, R. Ooka, Comparison of metaheuristic and linear programming models for the purpose of optimising building energy supply operation schedule, in: 12th REHVA World Congress, vol. 6, 2016.

Z. Pooranian, N. Nikmehr, S. Najafi-Ravadanegh, H. Mahdin, J. Abawajy, Economical and environmental operation of smart networked microgrids under uncertainties using NSGA-II, in: 2016 24th International Conference on Software, Telecommunications and Computer Networks (SoftCOM), IEEE, 1–6, 2016.

T. Prabatha, H. Karunathilake, A. M. Shotorbani, R. Sadiq, K. Hewage, Community-level decentralized energy system planning under uncertainty: A comparison of mathematical models for strategy development, Applied Energy 283 (2021) 116304.

V. Rasouli, I. Gonçalves, C. H. Antunes, Á. Gomes, A Comparison of MILP and metaheuristic approaches for implementation of a home energy management system under dynamic tariffs, in: 2019 International Conference on Smart Energy Systems and Technologies (SEST), IEEE, 1–6, 2019.

T. Rosfjord, W. Tredway, A. Chen, J. Mulugeta, T. Bhatia, Advanced microturbine systems, 2008.

T. Schütz, M. H. Schraven, M. Fuchs, P. Remmen, D. Müller, Comparison of clustering algorithms for the selection of typical demand days for energy system synthesis, Renewable energy 129 (2018) 570–582.

L. Schwartz, M. Wei, W. Morrow, J. Deason, S. R. Schiller, G. Leventis, S. Smith, W. L. Leow, T. Levin, S. Plotkin, et al., Electricity end uses, energy efficiency, and distributed energy resources baseline, Lawrence Berkeley National Laboratory, Energy Analysis and Environmental Impacts Division .

SciPy library, Continuous distributions in SciPy library in Python, https://docs.scipy.org/doc/scipy/reference/stats.html, accessed: 2021-02-04, 2019.

I. J. Scott, P. M. Carvalho, A. Botterud, C. A. Silva, Clustering representative days for power systems generation expansion planning: Capturing the effects of variable renewables and energy storage, Applied Energy 253 (2019) 113603.

M. Sengupta, Y. Xie, A. Lopez, A. Habte, G. Maclaurin, J. Shelby, The national solar radiation data base (NSRDB), Renewable and Sustainable Energy Reviews 89.

M. Sharifzadeh, H. Lubiano-Walochik, N. Shah, Integrated renewable electricity generation considering uncertainties: The UK roadmap to 50% power generation from wind and solar energies, Renewable and Sustainable Energy Reviews 72 (2017) 385–398.

F. Shen, L. Zhao, W. Du, W. Zhong, F. Qian, Large-scale industrial energy systems optimization under uncertainty: A data-driven robust optimization approach, Applied Energy 259 (2020) 114199.

C. L. B. Silveira, A. Tabares, L. T. Faria, J. F. Franco, Mathematical optimization versus Metaheuristic techniques: A performance comparison for reconfiguration of distribution systems, Electric Power Systems Research 196 (2021) 107272.

R. Sun, Y. Liu, H. Zhu, R. Azizipanah-Abarghooee, V. Terzija, A network reconfiguration approach for power system restoration based on preference-based multiobjective optimization, Applied Soft Computing 83 (2019) 105656.

Y. Sun, L. Gu, C. J. Wu, G. Augenbroe, Exploring HVAC system sizing under uncertainty, Energy and Buildings 81 (2014) 243–252.

V. S. Tabar, M. A. Jirdehi, R. Hemmati, Energy management in microgrid based on the multi objective stochastic programming incorporating portable renewable energy resource as demand response option, Energy 118 (2017) 827–839.

S. Taheri, I. Briggs, M. Burtscher, G. Gopalakrishnan, Difftrace: Efficient whole-program trace analysis and diffing for debugging, in: 2019 IEEE International Conference on Cluster Computing (CLUSTER), IEEE, 1–12, 2019.

S. Taheri, S. Devale, G. Gopalakrishnan, M. Burtscher, ParLOT: Efficient whole-program call tracing for HPC applications, in: Programming and Performance Visualization Tools, Springer, 162–184, 2017.

H. Teichgraeber, A. R. Brandt, Clustering methods to find representative periods for the optimization of energy systems: An initial framework and comparison, Applied energy 239 (2019) 1283–1293.

Tesla, Powerpack Utility and Business Energy Storage, https://www.tesla.com/powerpack/, accessed: 2021-10-28, 2021.

T. T. Tran, A. D. Smith, Stochastic optimization for integration of renewable energy technologies in district energy systems for cost-effective use, Energies 12 (3) (2019) 533.

K. Ullah, G. Hafeez, I. Khan, S. Jan, N. Javaid, A multi-objective energy optimization in smart grid with high penetration of renewable energy sources, Applied Energy 299 (2021) 117104.

University of Utah Sustainability and Energy Management, FY 2021 Utility Rates and Bill Collection Disbursement, https://facilities.utah.edu/sustainability-and-energy-management/resources/, accessed: 2021-07-20, 2020.

L. Urbanucci, D. Testi, Optimal integrated sizing and operation of a CHP system with Monte Carlo risk analysis for long-term uncertainty in energy demands, Energy conversion and management 157 (2018) 307–316.

U.S. Department of Energy, Combined Heat and Power Technology Fact Sheet Series, https://www.energy.gov/sites/prod/files/2016/09/f33/CHP-Microturbines_0.pdf, accessed: 2021-03-15, 2016.

U.S. Energy Information Administration, Utah Electricity Profile 2019, https://www.eia.gov/electricity/state/archive/2019/utah/, accessed: 2021-03-15, 2019.

U.S. Energy Information Administration, EIA-923: Annual State-level generation and fuel consumption data (back to 1990), https://www.eia.gov/electricity/data/state/annual_generation_state.xls, accessed: 26-01-2022, 2021.

U.S. Environmental Protection Agency, Emission Factors for Greenhouse Gas Inventories, https://www.epa.gov/sites/default/files/2020-04/documents/ghg-emission-factors-hub.pdf, accessed: 2021-03-15, 2020.

B. Van Der Heijde, A. Vandermeulen, R. Salenbien, L. Helsen, Representative days selection for district energy system optimisation: a solar district heating system with seasonal storage, Applied Energy 248 (2019) 79–94.

K. K. Wan, D. H. Li, D. Liu, J. C. Lam, Future trends of building heating and cooling loads and energy consumption in different climates, Building and Environment 46 (1) (2011) 223–234.

X. Wang, Z. Bie, F. Liu, Y. Kou, Co-optimization planning of integrated electricity and district heating systems based on improved quadratic convex relaxation, Applied Energy 285 (2021) 116439.

Y. Wang, Q. Hu, L. Li, A. M. Foley, D. Srinivasan, Approaches to wind power curve modeling: A review and discussion, Renewable and Sustainable Energy Reviews 116 (2019) 109422.

Wind turbine database, Osiris Energy and Endurance manufacturers, https://en.wind-turbine-models.com/, accessed: 2021-10-28, 2021.

R. Wu, G. Mavromatidis, K. Orehounig, J. Carmeliet, Multiobjective optimisation of energy systems and building envelope retrofit in a residential community, Applied Energy 190 (2017) 634–649.

T. Wu, S. Bu, X. Wei, G. Wang, B. Zhou, Multitasking multi-objective operation optimization of integrated energy system considering biogas-solar-wind renewables, Energy Conversion and Management 229 (2021) 113736.

C. Xu, Y. Ke, Y. Li, H. Chu, Y. Wu, Data-driven configuration optimization of an off-grid wind/PV/hydrogen system based on modified NSGA-II and CRITIC-TOPSIS, Energy Conversion and Management 215 (2020) 112892.

Y. Xu, G. Zhang, C. Yan, G. Wang, Y. Jiang, K. Zhao, A two-stage multi-objective optimization method for envelope and energy generation systems of primary and secondary school teaching buildings in China, Building and Environment (2021) 108142.

B. Yan, M. Di Somma, G. Graditi, P. B. Luh, Markovian-based stochastic operation optimization of multiple distributed energy systems with renewables in a local energy community, Electric Power Systems Research 186 (2020) 106364.

J. Yang, C. Su, Robust optimization of microgrid based on renewable distributed power generation and load demand uncertainty, Energy 223 (2021) 120043.

S. Yang, Z. Tan, Z. Liu, H. Lin, L. Ju, F. Zhou, J. Li, A multi-objective stochastic optimization model for electricity retailers with energy storage system considering uncertainty and demand response, Journal of Cleaner Production 277 (2020) 124017.

C. Yuan, H. Yang, Research on K-value selection method of K-means clustering algorithm, J—Multidisciplinary Scientific Journal 2 (2) (2019) 226–235.

Z. Ghaemi, A.D. Smith, Multi-objective optimization of Operation Planning, https://github.com/zahraghh/multi_objective_optimization/tree/Journal, 2021.

Z. Zhang, R. Jing, J. Lin, X. Wang, K. H. van Dam, M. Wang, C. Meng, S. Xie, Y. Zhao, Combining agent-based residential demand modeling with design optimization for integrated energy systems planning and operation, Applied Energy 263 (2020) 114623.

B. Zhao, J. Ren, J. Chen, D. Lin, R. Qin, Tri-level robust planning-operation co-optimization of distributed energy storage in distribution networks with high PV penetration, Applied Energy 279 (2020) 115768.

J. Zhong, Y. Tan, Y. Li, Y. Cao, Y. Peng, Z. Zeng, Y. Nakanishi, Y. Zhou, Distributed Operation for Integrated Electricity and Heat System With Hybrid Stochastic/Robust Optimization, International Journal of Electrical Power & Energy Systems 128 (2021) 106680.

S. Zhou, K. Sun, Z. Wu, W. Gu, G. Wu, Z. Li, J. Li, Optimized operation method of small and medium-sized integrated energy system for P2G equipment under strong uncertainty, Energy 199 (2020) 117269.

S. Zwickl-Bernhard, H. Auer, Open-source modeling of a low-carbon urban neighborhood with high shares of local renewable generation, Applied Energy 282 (2021) 116166.

Appendix

Table A.1: Energy prices and emission factors at University of Utah

Natural gas price \$/kWh	Electricity price \$/kWh	Natural gas EF kg-CO_2/kWh
0.01703	0.069	0.181048

Table A.2: Characteristics of natural gas boilers

Capacity kW	Thermal efficiency %	Investment cost \$/kW	Variable O&M cost \$/kWh
506.43	80	119.42	0.00324

Table A.3: Characteristics of the microturbine CHP system

Capacity kW	Total thermal efficiency ($\eta_{CHP,total}$) %	Electrical efficiency ($\eta_{CHP,elect}$)%	Investment cost \$/kW	Variable O&M cost \$/kWh
646	70.3	28.7	2560	0.008

Table A.4: Characteristics of the solar PV system

Solar area m^2	Tilt angle deg	Power density W/m^2	Module efficiency %	Inverter efficiency %	Investment cost \$/kW	Fixed O&M cost \$/kW-year	Variable O&M cost \$/kWh
7540	35	160	19.1	98	1830	18	0

Table A.5: Characteristics of the wind turbines

Rated power kW	Swept area m^2	Rated wind speed m/s	Cut-in wind speed m/s	Cut-off wind speed m/s	Investment cost \$/kW	Fixed O&M cost \$/kW-year	Variable O&M cost \$/kWh
6.4	32	10.5	2.4	25.0	1740	44	0

Table A.6: Characteristics of the batteries

Capacity kW	Charging efficiency %	Discharging efficiency %	Depth of discharge %	Investment cost \$/kW	Fixed O&M cost \$/kW-year	Variable O&M cost \$/kWh
54	85	85	90	2338	6	0